PLOS ONE

RESEARCH ARTICLE

Fusarium graminearum DICER-like-dependent sRNAs are required for the suppression of host immune genes and full virulence

Bernhard Timo Werner[1], Aline Koch[2], Ena Šečić[1], Jonas Engelhardt[1], Lukas Jelonek[3], Jens Steinbrenner[1], Karl-Heinz Kogel[1]*

1 Institute of Phytopathology, Centre for BioSystems, Land Use and Nutrition, Justus Liebig University, Giessen, Germany, **2** Institute for Phytomedicine, University of Hohenheim, Stuttgart, Germany, **3** Institute of Bioinformatics and Systems Biology, Justus Liebig University, Giessen, Germany

* Karl-Heinz.Kogel@agrar.uni-giessen.de

Citation: Werner BT, Koch A, Šečić E, Engelhardt J, Jelonek L, Steinbrenner J, et al. (2021) *Fusarium graminearum* DICER-like-dependent sRNAs are required for the suppression of host immune genes and full virulence. PLoS ONE 16(8): e0252365. https://doi.org/10.1371/journal.pone.0252365

Editor: Richard A Wilson, University of Nebraska-Lincoln, UNITED STATES

Received: May 11, 2021

Accepted: July 19, 2021

Published: August 5, 2021

Data Availability Statement: Data used in this study are available from the NCBI (Bioproject) repository at accession number: PRJNA749737 (https://www.ncbi.nlm.nih.gov/bioproject/PRJNA749737).

Funding: This work was supported by the Deutsche Forschungsgemeinschaft (www.dfg.de; Research Unit FOR5116) to KHK. BTW, AK, ES, JE, LJ and JS received no specific funding for this work. The funders had no role in study design, data

Abstract

In filamentous fungi, gene silencing by RNA interference (RNAi) shapes many biological processes, including pathogenicity. Recently, fungal small RNAs (sRNAs) have been shown to act as effectors that disrupt gene activity in interacting plant hosts, thereby undermining their defence responses. We show here that the devastating mycotoxin-producing ascomycete *Fusarium graminearum* (*Fg*) utilizes DICER-like (DCL)-dependent sRNAs to target defence genes in two Poaceae hosts, barley (*Hordeum vulgare*, *Hv*) and *Brachypodium distachyon* (*Bd*). We identified 104 *Fg*-sRNAs with sequence homology to host genes that were repressed during interactions of *Fg* and *Hv*, while they accumulated in plants infected by the DCL double knock-out (dKO) mutant PH1-*dcl1/2*. The strength of target gene expression correlated with the abundance of the corresponding *Fg*-sRNA. Specifically, the abundance of three tRNA-derived fragments (tRFs) targeting immunity-related *Ethylene overproducer 1-like 1* (*HvEOL1)* and three Poaceae orthologues of *Arabidopsis thaliana BRI1-associated receptor kinase 1* (*HvBAK1*, *HvSERK2* and *BdSERK2*) was dependent on fungal DCL. Additionally, RNA-ligase-mediated Rapid Amplification of cDNA Ends (RLM-RACE) identified infection-specific degradation products for the three barley gene transcripts, consistent with the possibility that tRFs contribute to fungal virulence via targeted gene silencing.

Introduction

RNA interference (RNAi) is a biological process in which small RNA (sRNA) molecules mediate gene silencing at the transcriptional or post-transcriptional level. In agriculture, RNAi-mediated silencing strategies have the potential to protect crops from pests and microbial pathogens [1–5]. Expression of non-coding double-stranded (ds) RNA targeting essential genes in a pest, a pathogen or a virus can render host plants more resistant by a process known as host-induced gene silencing (HIGS) [6–9]. Alternatively, plants can be protected by foliar application of dsRNA to plants [10–16]. While these RNAi-based crop protection strategies are

collection and analysis, decision to publish, or preparation of the manuscript.

Competing interests: The authors have declared that no competing interests exist.

proving to be efficient and agronomically practical in the control of insects [17] and viruses [18], many questions remain unanswered with regard to the control of fungi.

The blueprint for using RNA to fight disease comes from nature [7]. During infection of *Arabidopsis thaliana* (*At*), the necrotrophic ascomycete *Botrytis cinerea* (*Bc*) secretes DICER-like (DCL)-dependent sRNAs that are taken up into plant cells to interact with the Arabidopsis ARGONAUTE protein *At*AGO1 and initiate silencing of plant immune genes [19, 20]. For instance, sRNA *Bc*-siR3.2 targets mitogen-activated protein kinases, including *MPK2* and *MPK1* in *At*, and *MAPKKK4* in tomato (*Solanum lycopersicum*), while *Bc*-siR37 targets several immune-related transcription factors including *WRKY7*, *PMR6* and *FEI2* [21]. Likewise, the oomycete *Hyaloperonospora arabidopsidis* produces 133 AGO1-bound sRNAs, which are crucial for virulence [22], and microRNA-like RNA1 (*Pst*-milR1) from the yellow rust causing biotrophic basidiomycete *Puccinia striiformis* f.sp. *tritici* (*Pst*) reduced expression of the defence gene *Pathogenesis-related* 2 (*PR2*) in wheat (*Triticum aestivum*) [23]. Notably, when comparing sRNA in the leaf rust fungus *Puccinia triticina* (*Pt*), 38 *Pt*-sRNAs were homologous to sRNAs previously identified in *Pst* [24, 25], hinting to the possibility that sRNA effectors are conserved among related fungal species as it is known for plant miRNAs [26, 27]. One group of conserved sRNAs with putative effector function are transfer RNA (tRNA)-derived fragments (tRFs). Bacterial tRFs play a role in the symbiotic interaction between soybean (*Glycine max*) and its nitrogen fixing symbiont *Bradyrhizobium japonicum* during root nodulation [28]. Similarly, the protozoan pathogen *Trypanosoma cruzi* secretes tRF-containing microvesicles resulting in gene expression changes in mammalian host cells [29].

Fungal species of the genus *Fusarium* belong to the most devastating pathogens of cereals causing Fusarium head blight and crown rot [30], and contaminate the grain with mycotoxins such as the B group trichothecenes deoxynivalenol (DON), nivalenol (NIV), and their acetylated derivatives (3A-DON, 15A-DON, and 4A-NIV) [31–33]. Viability, aggressiveness, and virulence of Fusaria are under control of the RNAi machinery [8, 34, 35]. In tomato, a *Fol-milR1* produced by *F. oxysporum* f.sp. *lycopersici* (Fol) was shown to target the protein kinase *SlyFRG4* via AGO4a [36]. Moreover, in wheat, *Fg-sRNA1* produced by *Fg* targets and silences the pattern recognition receptor gene *TaCEBiP* (*Chitin Elicitor Binding Protein*) [37].

To further test the possibility of *Fg* producing sRNAs that exert effector function and promote pathogenesis, we predicted *Fg*-sRNA targets in two Poaceae hosts, *Hordeum vulgare* (*Hv*) and *Brachypodium distachyon* (*Bd*). Among the many predicted plant targets of fungal sRNA, three fungal tRFs had sequence similarity to *BRI1-associated receptor kinase 1* (*BAK1*) homologs and *EOL1* (*Ethylene overproducer 1-like 1*) in *Hv* and *Bd*. Upon infection with the wild type *Fg* strain, transcripts of genes were strongly reduced, while in contrast they were increased upon infection with *Fg* strains compromised for DCL activity. Degradation products of target mRNAs were detected by RNA-ligase-mediated Rapid Amplification of cDNA Ends (RLM-RACE), supporting the possibility that DCL-dependent sRNAs play a critical role in the interaction of *Fg* with cereal hosts.

Results

Fusarium graminearum DCL mutants are less virulent on barley and *Brachypodium* leaves

The *Fusarium* mutant IFA65-*dcl1* is partially impaired in infecting wheat ears and causing Fusarium Head Blight [8]. We extended this earlier study to examine the effects of impaired DCL activity on the plant defence response. To this end, two to three-week-old detached second leaves of barley cv. Golden Promise (GP) were drop-inoculated with 3 μl of a solution containing 150,000 conidia per ml of *Fg* isolate PH1 or the double knock-out (dKO) mutant

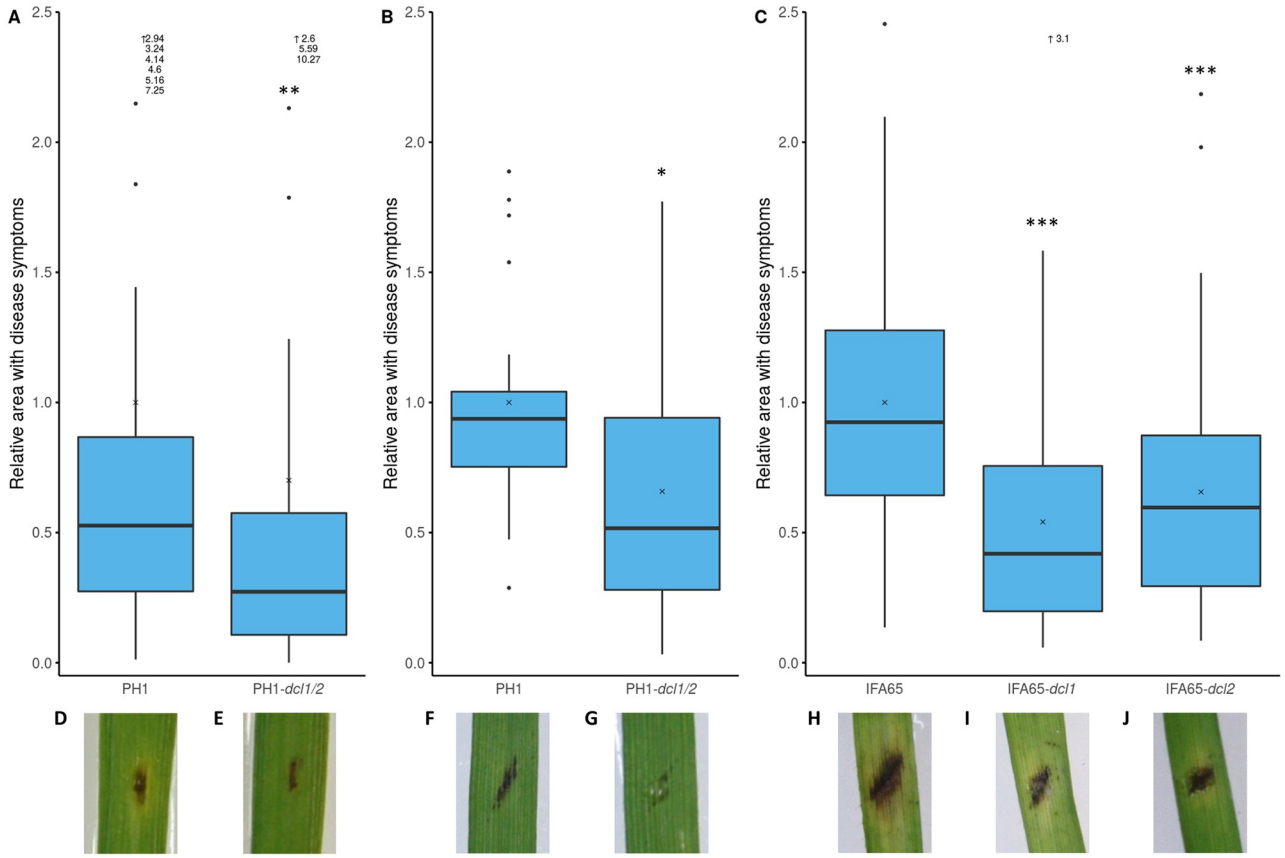

Fig 1. Virulence of *Fusarium graminearum* DCL single and dKO mutants on barley and *Brachypodium*. A: Relative infected area on leaves of barley cv. Golden Promise (GP) at 5 dpi. Detached leaves were inoculated with 3 μl of a solution containing 150,000 conidia per mL. The area with leaf necrosis was measured with the free image analysis software package PlantCV. Boxplots represent the median and quartiles of three independent biological experiments (n = 56). (Wilcoxon Rank Sum Test, $P = 7.1^{*}10^{-3}$, x = mean). B and C: Relative infected leaf area on leaves of *Brachypodium distachyon* Bd21-3 at 4 dpi (B) or 5 dpi (C). Detached leaves were inoculated with 10 μl of a solution containing 10,000 conidia per mL. The area with leaf necrosis was measured with ImageJ. Boxplots represent the median and quartiles of three (B) or nine (C) independent biological experiments (n = 21 (B), n = 63 (C)). (B: Wilcoxon Rank Sum Test, P = 0.013; C: Pairwise Wilcoxon Rank Sum Test, Bonferroni corrected, $P_{dcl1} = 4.9^{*}10^{-8}$, $P_{dcl2} = 2.6^{*}10^{-4}$; x = mean). Outliers (>2.5) are not shown but indicated as written values next to the upward arrow (↑). D-J: Representative pictures of disease symptoms of PH1 (D and F), PH1-*dcl1/2* (E and G), IFA65 (H), IFA65-*dcl1* (I) and IFA65-*dcl2* (J) on barley (D and E) and Bd (F-J).

https://doi.org/10.1371/journal.pone.0252365.g001

PH1-*dcl1/2*. At five days post inoculation (dpi), the dKO mutant produced significantly smaller necrotic lesions (30%; median (MED) (27%); interquartile range (IQR) (47%) Wilcoxon rank sum test, p = 0.007) than the wild type (wt) strain, confirming that DCL activity is required for full *Fg* virulence (Fig 1A).

Next, we determined the virulence of *DCL* mutants on *Brachypodium distachyon* Bd21-3. Flag leaves of three-week-old plants were inoculated with 10 μl (10,000 conidia ml^{-1}) of fungal inoculum. Single mutants IFA65-*dcl1* and IFA65-*dcl2* and dKO mutant PH1-*dcl1/2* produced significantly smaller lesions than the wt (PH1-*dcl1/2*, 66%; MED (52%); IQR (66%); Wilcoxon rank sum test; p = 0.013, IFA65-*dcl1*, 54%; MED (42%); IQR (56%) and IFA65-*dcl2*, 66%; MED (60%); IQR (58%); pairwise Wilcoxon rank sum test; Bonferroni corrected; $p<0.005$) (Fig 1B and 1C). These results substantiate the earlier findings [8] that fungal DCL activity is required for *Fusarium* virulence on graminaceous plants.

Selection of sRNAs with sequence homology to plant genes

We looked for interaction-related fungal sRNAs that potentially could interfere with plant gene expression by sequence-specific silencing. To this end, a previously published sRNA sequencing data set of *Fg* sRNAs from an axenic IFA65 culture [10] was analysed for sRNAs with sequence complementarity to barley genes. In order to identify a wide range of potential targets, we applied only two selection criteria, namely *i*. size (21–24 nt) and *ii*. a minimal number of reads (at least 400 reads in the dataset). From a total of 35,997,924 raw reads, 5,462,596 (comprising 589,943 unique sequences) had a length of 21–24 nt. From the unique sequences, 1,987 had at least 400 reads. Since the IFA65 genome has not been sequenced, we used the published genome information of *Fg* strain PH1 (genome assembly ASM24013v3 from International Gibberella zeae Genomics Consortium: GCA_000240135.3) for further analysis. The majority of the 1,987 unique sRNAs mapped to rRNA (64.4%) and intergenic regions (21.6%), while 3.7% and 2.4% mapped to protein coding genes and tRNAs, respectively, and 7.8% did not perfectly match the reference genome (S1 Fig). According to the TAPIR algorithm, the 1,987 sequences overall matched mRNAs of 2,492 genes (Hordeum vulgare IBSC PGSB v2 reference genome; [38]) sufficiently close according to the refined target prediction criteria suggested by Srivastava et al. [39]. GO-enrichment analysis revealed an enrichment in functions of nucleotide binding, motor activity and kinase activity and processes such as transport and localization (S2 Fig). Most of the 14,156 transcripts of the 2,492 target genes, which we nominated as potential sRNA targets, showed partially homologous sequences to more than one sRNA accounting for a total of 17,275 unique pairs of potential target gene—sRNA combinations. Target prediction results are presented with only one transcript (splice variant) for every combination (S1 Table). Of note, merely 101 out of the 1,987 sRNAs had no predicted target among the total number of 248,391 plant mRNAs in the IBSC_PGSB_v2 annotation.

Barley immune genes accumulate to higher levels in PH1-dcl1/2-infected leaves

From the set of 2,492 barley genes with partial sequence homology to *Fg* sRNAs, we selected 16 genes for further analysis, based on an educated guess that they are potentially involved in biotic stress reactions during plant-fungal interaction (Table 1). When tested with RT-qPCR, we found eight genes, being targeted by a total of 104 unique *Fg* sRNAs, significantly higher expressed (Student's *t*-test, paired, $^{*}p<0.1$, $^{**}p<0.05$, $^{***}p<0.01$) in leaves infected with PH1-*dcl1/2* vs. PH1 (Fig 2). Among these genes are three that encode proteins involved in the regulation of either ethylene (ET) (Ethylene overproducer 1-like 1, *Hv*EOL1) or auxin responses (Auxin response transcription factors *Hv*ARF10 and *Hv*ARF19) and three kinases, of which Somatic embryogenesis receptor-like kinase 2 (*Hv*SERK2) and BRI1-associated receptor kinase 1 (*Hv*BAK1) are likely involved in recognition of microbe-associated molecular patterns (MAMPs). Moreover, genes encoding the plastid kinase 2-Phosphoglycolate phosphatase 2 (*Hv*PGLP2), Resurrection 1 (*Hv*RST1, with a rather elusive function in cuticle formation and embryo development), and the histone-lysine N-methyltransferase Su(var)3-9-related protein 5 (*Hv*SUVR5, involved in transcriptional gene silencing) were also strongly expressed.

The first column gives the name of the respective gene abbreviated as in Fig 1 and in full. The second column shows the respective accession. In the third column selected GO terms are shown. The fourth and fifth columns give the accession and abbreviated name of the closest homologue in *At*.

Table 1. Selected GO-terms of tested genes and closest homologs in *A. thaliana*.

Name	ensembl_gene_id	GO_term	*A.thaliana* Homolog	Abbr.
HvARF3	HORVU1Hr1G076690	auxin-activated signaling pathway	AT2G33860	*ARF3*
Auxin response transcription factor 3		regulation of transcription, DNA-templated		
		nucleus		
HvSUB1	HORVU2Hr1G028070	Golgi apparatus	AT4G08810	*SUB1*
Short under blue light 1		transferase activity, transferring glycosyl groups		
		fucose metabolic process		
HvPPR	HORVU2Hr1G078260	protein binding	AT2G06000	
Pentatricopeptide repeat superfamily protein				
HvSERK2	HORVU2Hr1G080020	integral component of membrane	AT1G34210	*SERK2*
Somatic embryogenesis receptor-like kinase 2_1		positive regulation of innate immune response		
		regulation of defense response to fungus		
HvARF10	HORVU2Hr1G089670	auxin-activated signaling pathway	AT2G28350	*ARF10*
Auxin response transcription factor 10		regulation of transcription, DNA-templated		
		nucleus		
HvEOL1	HORVU2Hr1G119180	regulation of ethylene biosynthetic process	AT4G02680	*EOL1*
ETO1-like 1		protein binding		
HvRST1	HORVU3Hr1G016630	integral component of membrane	AT3G27670	*RST1*
Resurrection 1		membrane		
HvPIX7	HORVU3Hr1G051080	protein serine/threonine kinase activity	AT5G15080	*PIX7*
Putative interactor of XopAC 7		ATP binding		
		protein kinase activity		
Hvemb2726	HORVU5Hr1G024470	translation elongation factor activity	AT4G29060	*emb2726*
Embryo defective 2726		mitochondrion		
		intracellular		
HvPGLP2	HORVU5Hr1G052320	chloroplast	AT5G47760	*PGLP2*
2-Phosphoglycolate phosphatase 2		phosphoglycolate phosphatase activity		
		hydrolase activity		
HvATG2	HORVU6Hr1G034660	autophagy of peroxisome	AT3G19190	*ATG2*
Autophagy-related 2		autophagy		
HvSUVR5	HORVU6Hr1G069350	histone-lysine N-methyltransferase activity	AT2G23740	*SUVR5*
Su(var)3-9-related protein 5		chromosome		
		methyltransferase activity		
HvRDR1	HORVU6Hr1G074180	RNA-directed 5'-3' RNA polymerase activity	AT1G14790	*RDR1*
RNA-dependent RNA polymerase 1		RNA binding		
		gene silencing by RNA		
HvGDH	HORVU6Hr1G076880	glycine decarboxylation via glycine cleavage system	AT2G35370	*GDH1*
Glycine decarboxylase complex H		glycine cleavage complex		
		mitochondrion		
HvBAK1	HORVU7Hr1G068990	integral component of membrane	AT1G34210	*SERK2*
Somatic embryogenesis receptor-like kinase 2_2		transmembrane receptor protein serine/threonine kinase signaling pathway		
HvARF19	HORVU7Hr1G096460	auxin-activated signaling pathway		
Auxin response transcription factor 19		regulation of transcription, DNA-templated		
		nucleus		
BdSERK2	BRADI_5g12227v3	integral component of membrane	AT1G34210	*SERK2*
Somatic embryogenesis receptor-like kinase 2		positive regulation of innate immune response		
		regulation of defense response to fungus		

https://doi.org/10.1371/journal.pone.0252365.t001

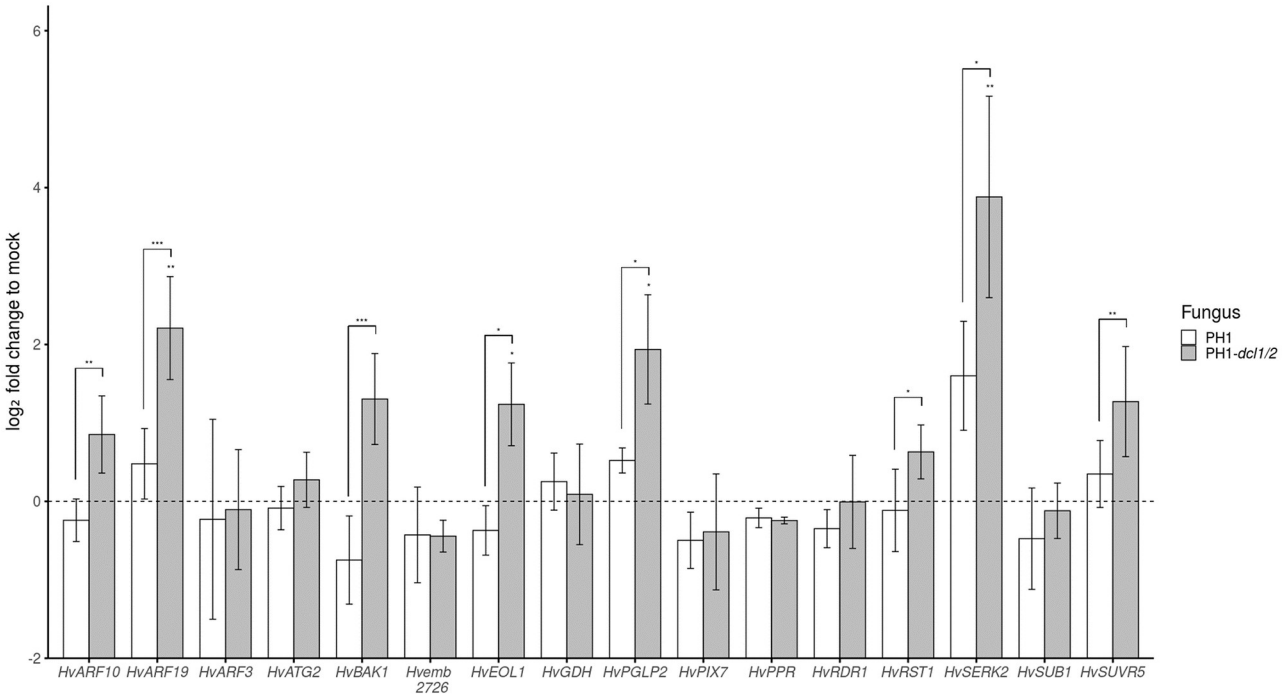

Fig 2. Relative expression (log2 fold) of potential barley target genes for fungal sRNAs in leaves infected with *Fusarium graminearum* wt strain PH1 vs. PH1-dcl1/2. Expression was normalized against barley *Ubiquitin* (*HvUBQ*) and subsequently against the Δct of the uninfected control (mock treatment). Bars represent the mean±SE of three independent biological replicates. Significant differences were calculated for the expression of a respective gene in PH1 vs. PH1-*dcl1/2*-infected samples and PH1 vs. controls. The dotted line shows the expression level of mock treatment. (Student's *t*-test, (paired) one sided, $^{*}P<0.1$, $^{**}P<0.05$, $^{***}P<0.01$).

https://doi.org/10.1371/journal.pone.0252365.g002

HvEOL1 transcripts also accumulate to higher levels upon DCL knock-down via spray induced gene silencing (SIGS)

We selected *HvEOL1* (*HORVU2Hr1G119180*), which is a homologue of *At Ethylene overproducer1* (*AtETO1*; *AT4GO2680.1*), for further analysis. The alignment of the respective protein sequences of *Hv*EOL1 and *At*ETO1 is shown in S3 Fig. *At*ETO1 negatively regulates ethylene synthesis in *At* by ubiquitination of type-2 1-Aminocyclopropane-1-carboxylate synthases (ACSs), which produce the direct precursor of ET [40] (S4 Fig). Upon inoculation with PH1, *HvEOL1* expression was reduced by 23% as compared to non-inoculated barley leaves. In contrast, *HvEOL1* was strongly expressed in PH1-*dcl1/2*-infected leaves well above the levels measured either in PH1- or mock-inoculated leaves. To further substantiate that *HvEOL1* expression is under the control of fungal DCL activity, we used a SIGS strategy [10] to partially inactivate DCL function in *Fg*. Two-week-old detached leaves were sprayed with 20 ng μl^{-1} of dsRNA-*dcl1/2*, a 1,782 nt long dsRNA derived from the sequences of IFA65-*DCL1* and IFA65-*DCL2* (S5A and S5B Fig). 48 h later, leaves were drop inoculated with conidia and harvested at 5 dpi. Consistent with the expectation that exogenous dsRNA-*dcl1/2* mediates silencing of their *DCL* gene targets, RT-qPCR analysis confirmed that the transcript levels of IFA65-*DCL1* and IFA65-*DCL2* were reduced to 22% and 42%, respectively, as compared with the Tris-EDTA (TE) buffer control (Fig 3A). In accordance with the results obtained with strain PH1, *HvEOL1* was also significantly ($p = 0.029$, Student's *t*-test (Δct), one sided, paired) downregulated in response to IFA65 infection compared to mock controls treated with 0.02% Tween20 (Fig 3B). In contrast, however, when leaves were sprayed with dsRNA-*dcl1/2* prior to

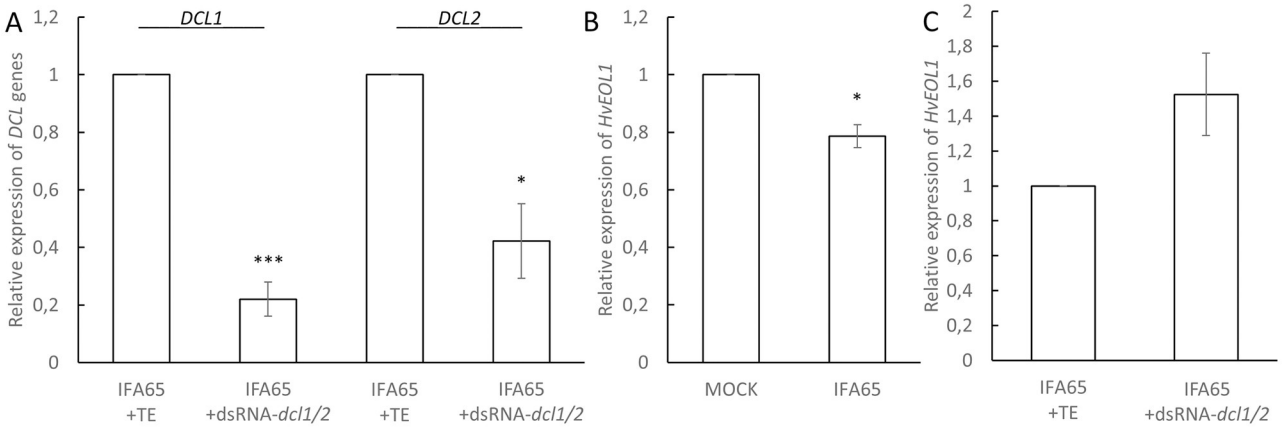

Fig 3. Relative expression of HvEOL1 in response to inoculation of barley leaves with *Fusarium graminearum*. A, Relative expression of *FgDCL1* and *FgDCL2* on detached barley cv. Golden Promise leaves at 5 dpi in wt strain IFA65 and 7 days post spray application of the 1,782 nt long dsRNA construct dsRNA-*dcl1/2* vs. TE buffer. **B**, Relative expression of *HvEOL1* at 5 dpi with IFA65 vs. mock control. **C**, Relative expression of *HvEOL1* 5 dpi with wt strain IFA65 and 7 days post spray application of dsRNA-*dcl1/2* vs. TE buffer. Gene expression was first normalized against the reference gene *HvUBQ (HORVU1Hr1G023660)* and subsequently against the Δct of the respective control for B (mock = 0.002% Tween20) and for A,C (IFA65 / TE). Bars represent the mean ± SE of three (B) and four (A, C) independent biological replicates. (Student's *t*-test, $^{*}P<0.05$, $^{***}P<0,005$).

https://doi.org/10.1371/journal.pone.0252365.g003

inoculation with IFA65, *HvEOL1* transcripts accumulated (p = 0.055, Student's *t*-test (Δct), one sided, paired) in comparison with the inoculated leaves sprayed with TE buffer (Fig 3C).

Fungal sRNAs targeting HvBAK1, HvEOL1, and HvSERK2 mRNAs are less abundant in PH1-dcl1/2 vs. PH1

To detect the abundance of specific *Fg*-sRNAs, originally identified by sequencing of axenic IFA65 mycelium, in PH1-infected plant tissue, we performed reverse transcription stem-loop qPCR [41]. From the above defined pool of 1,987 *Fg*-sRNAs (axenic, 21–24 nt length, > = 400 reads) 22 unique sRNAs matched partial sequences of *HvEOL1*, 10 matched *HvBAK1* and five matched *HvSERK2*. *Fg*-sRNA-1921 matched all three genes and *Fg*-sRNA-321 matched both *HvEOL1* and *HvBAK1* (Table 2 and S2 Table). These two sRNAs show high sequence similarities among each other. To identify their origin, they were aligned to the genomic sequence of strain PH1 (GCA_900044135.1). We found that they match the gene *Fg_CS3005_tRNA-Gly-GCC-1-9* encoding tRNA-Gly for the anticodon GCC. Of note, a larger cluster of 27 overlapping tRNA-derived fragments (tRFs) with more than 50 reads matching the tRNA-Gly gene sequence were detected (S6 Fig). To assess differential accumulation of tRFs from the *Fg_CS3005_tRNA-Gly-GCC-1-9* cluster in leaves infected with PH1 *vs*. PH1-*dcl1/2*, sRNAs were reverse transcribed using hairpin-priming followed by qPCR amplification [41]. For this analysis, we chose *Fg*-sRNA-321, the most abundant tRF from this cluster, along with *Fg*-sRNA-1921, which targets all three GOIs and an additional tRF (*Fg*-sRNA-6717), which targets *HvEOL1* and *HvBAK1* (see Table 2) to assess the sensitivity of the assay. In the initial IFA65 dataset the *Fg*-sRNA-321 had a read count of 2,106, *Fg*-sRNA-1921 had 416 and *Fg*-sRNA-6717 had 86 from a total of more than 5 million reads (S7 Fig). This equals 386 reads per million (rpm) for *Fg*-sRNA-321, while in average unique reads had only 1.7 rpm. Using TAPIR [42], we also calculated the target score values for all three tRFs, which is a measure for the similarity between sRNA and target. A high value refers to more dissimilarities. Mismatches (MMs) increase the score by one point and G-U pairs by 0.5 points. These values are doubled if the respective MMs and G-U pairs are located between the second and 12th nt of the sRNA

Table 2. Target prediction results of *Fg*-sRNAs with more than 400 reads in IFA65 axenic culture.

sRNA-Name	Reads	Score	Alignment			Length
Fg-sRNA-321	2106	4.5	3'	GCUUGGGUCCCGAGGGGCUACC	5'	22
				..|.o||||||||||o|||		
HvEOL1			5'	GAAUUCCAGGGCUCCCCGGUGG	3'	
Fg-sRNA-1921	416	3.5	3'	CUUGGGUCCCGAGGGGCUACC	5'	21
				.|.o||||||||||o|||		
HvEOL1			5'	AAUUCCAGGGCUCCCCGGUGG	3'	
Fg-sRNA-6717	86	4.5	3'	UAGCUUGGGUCCCGAGGGGCUAC	5'	23
				||..|.o||||||||||o||		
HvEOL1			5'	AUGAAUUCCAGGGCUCCCCGGUG	3'	
Fg-sRNA-1921	416	6	3'	CUUGGGUCCCGAGGGGCUACC	5'	21
				|.||.||||.||.|||||||		
HvSERK2			5'	GCACGCAGGGGUCACCGAUGG	3'	
Fg-sRNA-321	2106	4.5	3'	GCUUGGGUCCCGAGGGGCUACC	5'	22
				o|.||.|||||||||.||||		
HvBAK1			5'	UGCACACAGGGCUCCCCCAUGG	3'	
Fg-sRNA-1921	416	4	3'	CUUGGGUCCCGAGGGGCUACC	5'	21
				|.||.|||||||||.||||		
HvBAK1			5'	GCACACAGGGCUCCCCCAUGG	3'	
Fg-sRNA-6717	86	5.5	3'	UAGCUUGGGUCCCGAGGGGCUAC	5'	23
				.|o|.||.|||||||||.|||		
HvBAK1			5'	UUUGCACACAGGGCUCCCCCCAUG	3'	
Fg-sRNA-321	2106	5.5	3'	GCUUGGGUCCCGAGGGGCUACC	5'	22
				..|.o||||||||o|||o|||		
BdEOL1			5'	GAAUUCCAGGGCUCUCCGGUGG	3'	
Fg-sRNA-1921	416	4.5	3'	CUUGGGUCCCGAGGGGCUACC	5'	21
				.|.o||||||||o|||o|||		
BdEOL1			5'	AAUUCCAGGGCUCUCCGGUGG	3'	
Fg-sRNA-6717	86	5.5	3'	UAGCUUGGGUCCCGAGGGGCUAC	5'	23
				||..|.o||||||||o|||o||		
BEOL1			5'	AUGAAUUCCAGGGCUCUCCGGUG	3'	
Fg-sRNA-321	2106	3.5	3'	GCUUGGGUCCCGAGGGGCUACC	5'	22
				o|.||.||.||||||||||		
BdSERK2			5'	UGCACGCAAGGCUCCCCGAUGG	3'	
Fg-sRNA-1921	416	3	3'	CUUGGGUCCCGAGGGGCUACC	5'	21
				|.||.||.||||||||||		
BdSERK2			5'	GCACGCAAGGCUCCCCGAUGG	3'	
Fg-sRNA-6717	86	5.5	3'	UAGCUUGGGUCCCGAGGGGCUAC	5'	23
				..o|.||.||.||||||||||		
BdSERK2			5'	UCUGCACGCAAGGCUCCCCGAUG	3'	

Mismatches (MMs) between mRNA and sRNA are marked as ".", while G-U pairs are marked as "o".

https://doi.org/10.1371/journal.pone.0252365.t002

(5'-3') because a high similarity in the seed region of the sRNA is especially important for RNAi [43]. *Fg*-sRNA-321 has a score of 4.5 for *HvBAK1* and *HvEOL1*, *Fg*-sRNA-1921 has a score of 4, 3.5 and 6 for *HvBAK1*, *HvEOL1* and *HvSERK2*, respectively and *Fg*-sRNA-6717 has a score of 5.5 and 4.5 with *HvBAK1* and *HvEOL1*. In plants other than Arabidopsis, such as

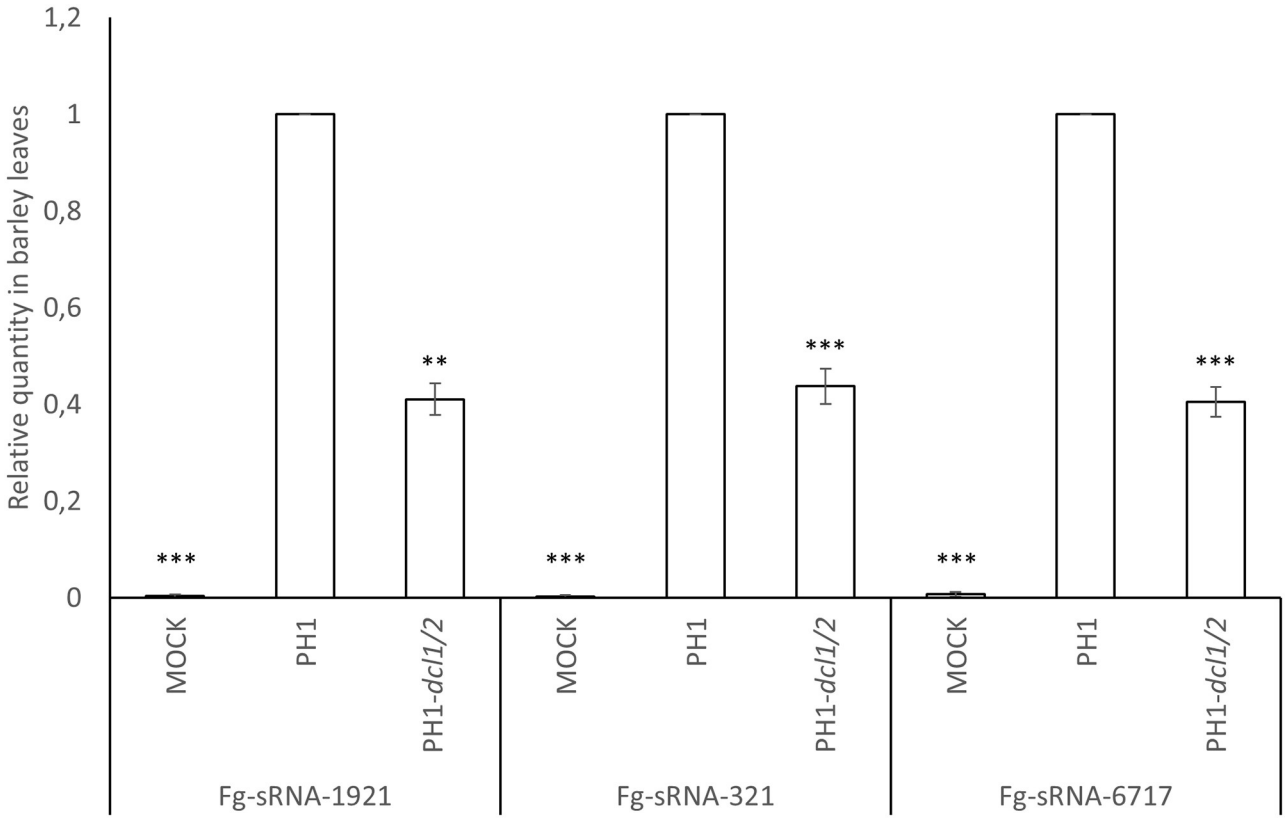

Fig 4. Relative amount of different fungal tRFs with homology to *HvEOL1* mRNA. Relative amount of different fungal tRFs with homology to *HvEOL1* mRNA during infection of barley leaves with PH1 and PH1-*dcl1/2* normalized to fungal biomass and relative quantity of sRNAs normalized to wt PH1 measured by qPCR. *Fg*-sRNA-1921, *Fg*-sRNA-321 and *Fg*-sRNA-6717 quantity was normalized to *Hvu*-miR159 and *Hvu*-miR168 and fungal biomass as determined by *FgEF1α* expression was normalized to *HvUBQ*. Subsequently the amount of sRNAs was normalized with fungal biomass. The amount of sRNA in PH1-infected leaves was set to 1. Values and error bars represent the mean ± SE of three independent biological replicates. Significance was calculated via a one-sample *t*-test. (**P<0.01, ***P<0.005).

https://doi.org/10.1371/journal.pone.0252365.g004

wheat and rice, a score cut off at 4 or 6 points lead to a precision of 82% or 62% and a recall of known interactions of 39% or 58% respectively according to Srivastava et al. [39].

All three fungal tRFs were detected in infected leaves, while they could not be found in uninfected leaves (Fig 4). Significantly lower amounts of *Fg*-sRNA-1921 (59%), *Fg*-sRNA-321 (56%), and *Fg*-sRNA-6717 (60%) were detected in PH1-*dcl1/2 vs*. PH1-infected leaves (Fig 4), showing that their biogenesis is DCL-dependent.

Fg-sRNA-321 and *Fg*-sRNA-1921 also match *SERK2* in *Brachypodium distachyon* Bd21-3

Next, we assessed the possibility that *Fg*-sRNA-321, *Fg*-sRNA-1921 and *Fg*-sRNA-6717 also have sequence homologies in *At* and the model grass *Bd*. Target prediction with the TAPIR algorithm using the optimised parameters for *At* (score = 4; mfe = 0.7), could not detect potential targets in *At* ecotype Col-0. In contrast, these three tRFs matched the sequence of *Brachypodium somatic embryogenesis receptor-like kinase 2* (*BdSERK2*) in Bd21-3 with a score of 3.5, 3 and 5.5, respectively (Table 2). We examined the expression pattern of *BdSERK2* in response to leaf infection: *BdSERK2* is relatively weakly expressed in uninfected plants and is not further suppressed after inoculation with PH1, whereas it strongly accumulated in PH1-*dcl1/2 vs*.

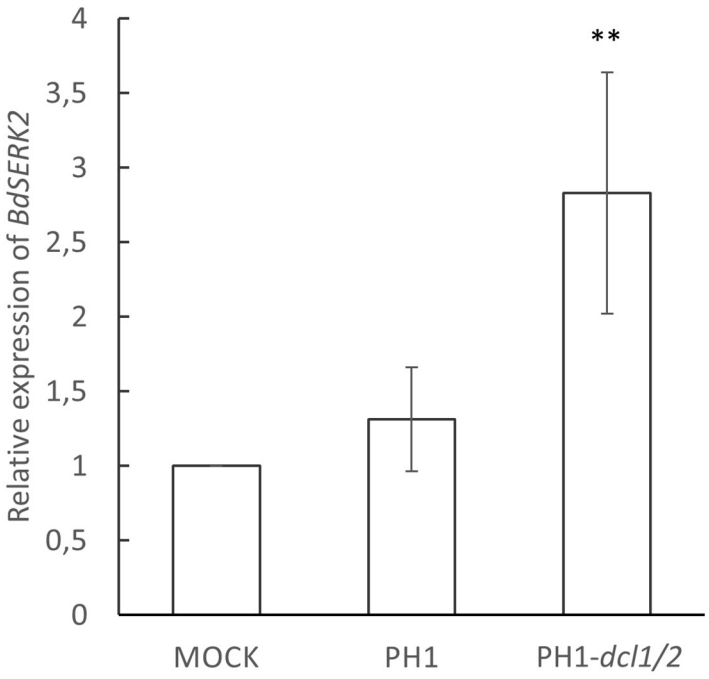

Fig 5. Relative expression of BdSERK2 in response to inoculation of *Brachypodium distachyon* leaves with *Fusarium graminearum*. Relative expression of *BdSERK2* in detached Bd21-3 leaves at 4 dpi with PH1 vs. PH1-*dcl1/2*. The gene expression was first normalized against the reference gene *BdUBI4* and subsequently against the Δct of the mock treated control. Values and error bars represent the mean ± SE of three independent biological replicates. (Student's t-test, paired, one sided, $^{**}P<0{,}01$).

https://doi.org/10.1371/journal.pone.0252365.g005

PH1-infected Bd21-3 (Fig 5). This finding further supports the possibility that the control of *SERK2* expression via RNAi pathways by *Fg* is evolutionary conserved in cereals.

RLM-RACE shows infection specific degradation products of *HvBAK1*, *HvEOL1* and *HvSERK2*

We assessed the sRNA-mediated cleavage of *HvBAK1*, *HvEOL1*, and *HvSERK2* mRNAs, using a modified RNA-ligase-mediated Rapid Amplification of cDNA Ends (RLM-RACE) assay. Control samples were prepared both from uninfected tissue and from infected tissue without the reverse transcription step (no-RT control) and PCR products were visualized on an EtBr-Agarose gel. In these no-RT controls no amplification was visible.

For each gene more than one infection-specific product was amplified (blue and red arrows), which could not be amplified from the uninfected sample (Fig 6D–6F). We excised three bands (red arrows) of the expected size for a *Fg*-sRNA-1921 guided cleavage of *HvBAK1* (Fig 6D) and one band for *HvEOL1* (Fig 6E) and *HvSERK2* (Fig 6F) and cloned them into the pGEM-T easy vector system. According to the IBSC_PGSB_v2 assembly, *HvBAK1* has splice variants, which could produce cleavage products of different lengths while for *HvSERK2* and *HvEOL1* there are no introns between sRNA target site and primer. From each band, five colonies were picked and for 23 of these extracted plasmids sequences were obtained. 16 sequences perfectly matched the reference genome, four with one MM and one with four MMs. Two sequences did not match the reference sufficiently enough to be aligned over the full length. The observed cleavage products are close to but do not match the canonical slice site between the 10^{th} and 11^{th} nt of *Fg*-sRNA-1921 and *Fg*-sRNA-321 (Fig 6A–6C).

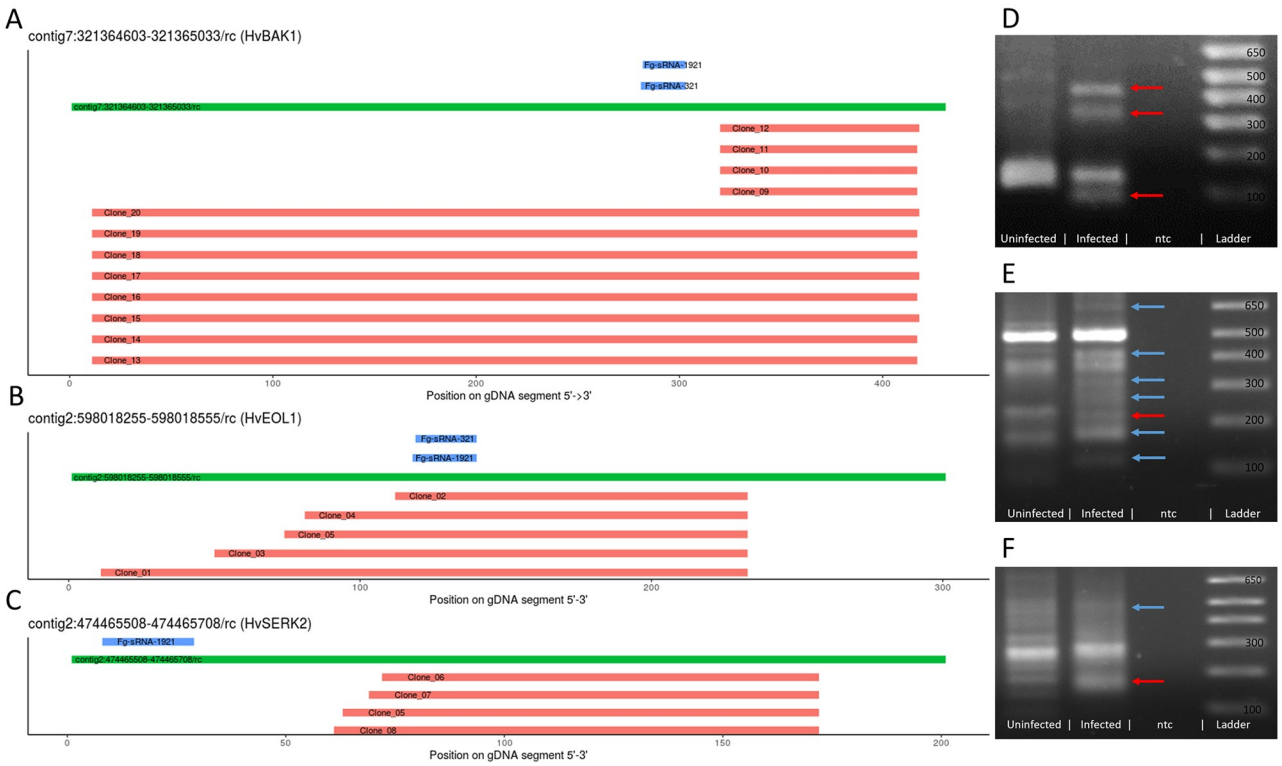

Fig 6. Analysis of potential target sites of *Fg*-sRNAs as determined by RLM-RACE products. A,B,C Potential target sites of *Fg*-sRNA-321 and *Fg*-sRNA-1921 predicted by TAPIR (blue), genomic DNA (GPv1, GCA_902500625.1, A: contig7:321364603–321365033, B: contig2:598018255–598018555, C: contig2:474465508–474465708) of barley cv. Golden Promise (green), and the alignment of sequences derived from the RLM-RACE PCR (red) relative to the *Hv*-gDNA and *Fg*-sRNAs. **D,E,F** PCR-products of the second nested RLM-RACE-PCR visualized in an EtBr-Agarose gel. Red arrows indicate excised bands and blue arrows indicate infection specific products.

https://doi.org/10.1371/journal.pone.0252365.g006

Total sRNAs predicted to target a gene in barley are correlated with the de-repression strength

Not all potential targets of *Fg*-sRNAs are downregulated nor do all potential targets show a re-accumulation upon infection with PH1-*dcl1/2* (see Fig 3). To address this bias we conducted a more focused target prediction exclusively for the 16 genes already tested by RT-qPCR. This allowed a much more thorough search, where targets for all sRNAs with at least two reads were predicted. From these 136,825 unique sRNAs (axenic, 21–24 nt length, > = 2 reads) representing 4,997,312 reads of the total of 5,439,472 reads 21–24 nt in length, 5,052 have potential target sequences in the 16 mRNA sequences selected for further investigation in the *Hordeum vulgare* cv. GP assembly GCA_902500625. An additional filter step was employed to select for sRNAs with a maximum of one MM to the PH1 assemblies GCA_000240135.3 and GCA_900044135.1. Subsequently, sRNAs with up to one MM to *Fg*-rRNAs were removed leaving a total of 1,212 sRNAs with 1,311 potential sRNA-mRNA interactions representing 85,531 reads in the analysis.

To establish a correlation of the observed resurgence of potential target genes and targeting sRNAs, we analysed the *DCL*-dependent expression change using ΔΔΔct values. To compare the expression of a GOI in two samples, the difference between the ct-values for a reference gene and the GOI can be determined (Δct) and to calculate the expression difference between the control and treated sample the difference between the Δct values (ΔΔct) is calculated. We

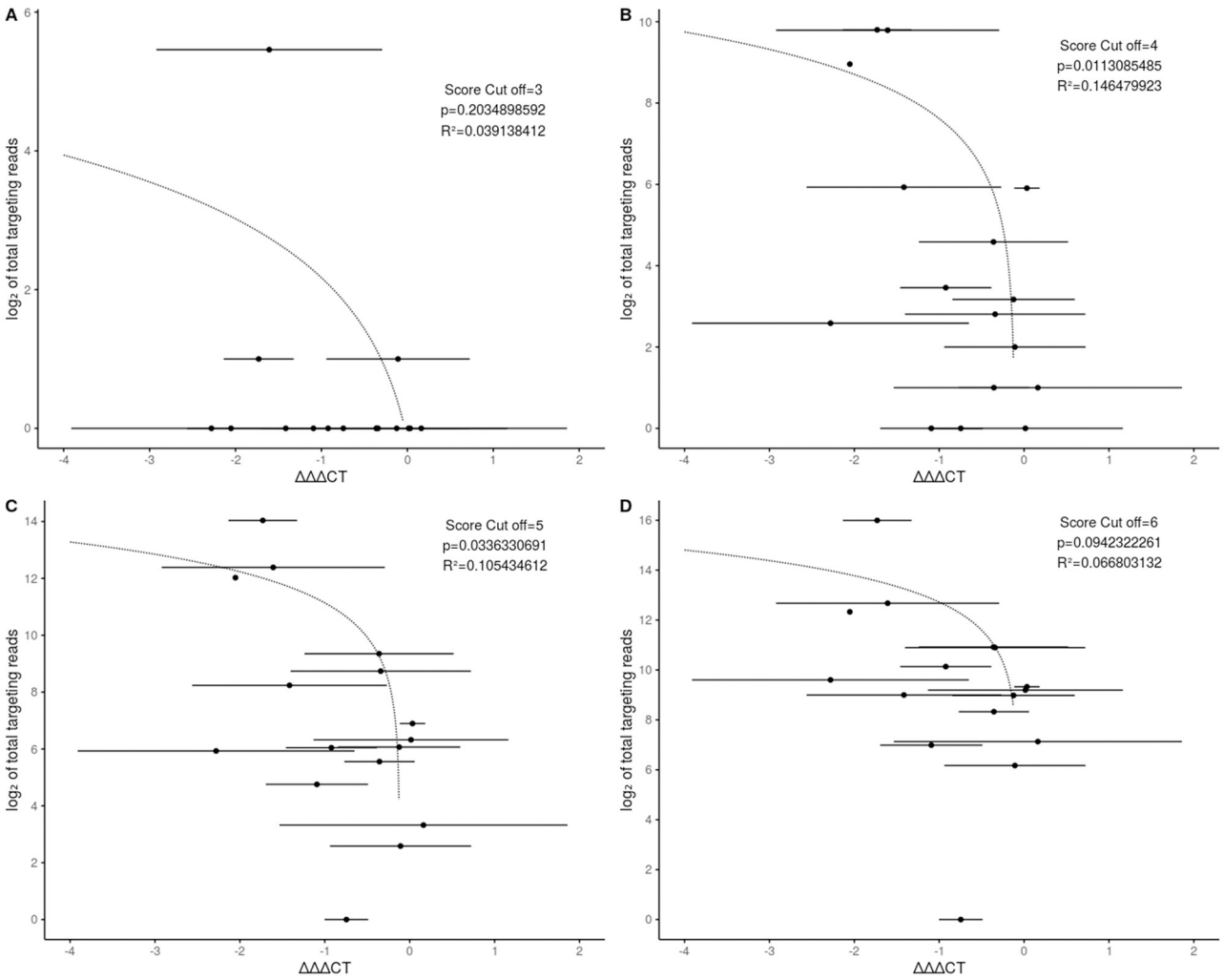

Fig 7. The degree of DCL-dependent gene silencing is correlated with the number of homologous fungal sRNAs. Each dot represents a predicted target gene of *Fg*-sRNAs. On the x-axis the ΔΔΔct-value is shown with bars representing SD. On the y-axis the $\log_2$ of the number of total sRNAs potentially targeting each gene are shown. The dotted line represents a linear regression model. P indicates the significance (t-test) of the model and the score cut-off indicates the score limit used during the target prediction. Plot A, B, C and D are the calculations for a score cut off of 3, 4, 5 and 6 respectively.

https://doi.org/10.1371/journal.pone.0252365.g007

further defined the ΔΔΔct value as the difference between the ΔΔct values for a GOI in PH1 and PH1-*dcl1/2*-infected samples. From this follows a gene with a negative ΔΔΔct value shows a higher transcript accumulation during the infection with a fungal strain with compromised DCL function and the stronger the accumulation the lower this ΔΔΔct value is. We found a negative correlation between the ΔΔΔct value and the number of total sRNAs targeting a GOI (Fig 7). This correlation becomes more significant if a lower score cut-off for the target prediction is chosen until the cut-off of four. The most significant correlation is for all predicted interactions with a score equal or below four with a p-value of 0.011 (t-test) (Fig 7B). The p-value for a correlation with a cut-off of five (Fig 7C) is 0.033 (t-test) and six (Fig 7D) is 0.094 (t-test), while a score cut-off of 3 leads to a situation, where there are no predicted sRNA interactions for all genes except for three (Fig 7A).

Discussion

We show here that full virulence of the ascomycete fungus *Fusarium graminearum* on graminaceous leaves depends on the activity of fungal DCLs. The dKO mutant PH1-*dcl1/2* is less virulent on barley and the two single KO mutants IFA65-*dcl1* and IFA65-*dcl2* also are less virulent on *Brachypodium*. These results are consistent with our previous studies showing that knock-down or SIGS-mediated silencing of *Fusarium DCLs* and other components of the RNAi machinery reduced the virulence of the fungus on barley [8, 44]. DCL enzymes are key components of the fungal RNAi machinery required for the biogenesis of sRNAs directing silencing of sequence-complementary endogenous and foreign genes [45]. The latter case involves DCL-dependent pathogen-derived sRNAs that target plant defense genes to increase virulence as shown for *Botrytis cinerea* [19, 21], *Puccinia striiformis* [23] and *Magnaporthe oryzae* [46].

In the present work we found potential host target genes for fungal small RNAs (*Fg*-sRNAs) that were differentially regulated in response to plant infection with *Fg* wt *vs*. *Fg* DCL KO mutants, and the same effect was confirmed when DCLs were silenced by SIGS. This suggests a scenario in which impaired DCL function resulting in reduced fungal RNAi activity ultimately leads to de-repression of host target genes. Of note, target gene de-repression was also observed when the transcript was not significantly downregulated by the wt fungus during infection. This could be explained by a mutually neutralizing effect in which *Fg*-sRNAs continuously target genes for silencing, while concurrent plant immune responses are a trigger for up-regulation. Thus, one can speculate that these described effects reflect an abrogation of host-favouring upregulation by host immunity *vs*. pathogen-favouring downregulation by sRNA effectors.

We identified three tRFs predicted to target *BdSERK2*, *HvBAK1*, *HvEOL1* and *HvSERK2*. Unexpectedly, these tRFs are partially DCL-dependent, with a reduced abundance by more than 50% during infections with the dKO mutant PH1-*dcl1/2 vs*. wt PH1 based on fungal biomass. Current knowledge of tRFs in fungi and oomycetes suggests that their silencing activity is independent of DCL, as shown for *Sclerotinia sclerotiorum* [47] and *Phytophthora infestans*, where the production is partially dependent on AGO [48]. Furthermore, analysis of tRFs in Cryptococcus spp. revealed a RNAi-independent generation of tRFs and possible compensatory effects in an RNAi-deficient genotype [49]. Interestingly however, the tRFs *Fg*-sRNA-321, *Fg*-sRNA-1921 and *Fg*-sRNA-6717 are neither 5'- or 3' tRNA halves nor do they belong to any of the described tRF-1, tRF-2, tRF-4 or tRF-5 classes [50] applied by the tRFtarget database for animals, yeast (*Schizosaccharomyces pombe*) and the bacterium *Rhodobacter sphaeroides* [51]. When following the classification of the tsRBase used for all eukaryotic kingdoms and bacteria [52], the three tRFs are classified as internal tRFs based on the origin within the mature tRNA. Interestingly, there are tRFs found in *Phytophthora sojae* starting in the anticodon loop and ending in the T loop of mature tRNAs [53], which resembles the Fg-sRNA tRFs (S8 Fig).

We observed several infection-specific degradation products of the predicted host target genes *HvBAK1*, *HvEOL1* and *HvSERK2* for tRFs *Fg*-sRNA-321, *Fg*-sRNA-1921 and *Fg*-sRNA-6717. However, cleavage occurred outside the canonical miRNA cleavage site as defined by Mallory et al. [43], though these genes are partially silenced during infection and silencing is apparently abolished upon infection with the DCL dKO mutant. While the canonical cleavage site for miRNA-directed cleavage in *At* is well defined, the tRF-directed cleavage observed by 5' RACE of transposable elements in *At* [54] and of defence-related genes during the infection of black pepper (*Piper nigrum*) with *Phytophthora capsici* [55] was found outside of the canonical cleavage site. Additionally, the identification of sRNA-directed cleavage sites in barley often leads to divergent findings. Ferdous et al. [56] predicted ~400 target genes for 11

presumably drought responsive miRNAs and found cleavage products for 15 targets overlapping the respective miRNAs alignment through degradome sequencing in the two barley cultivars Golden Promise (GP) and Pallas. From these confirmed targets, 13 were cleaved at the canonical 10^{th}-11^{th} nt site, one was cleaved at 19^{th}-20^{th} nt, and one at the 5^{th}-6^{th} nt. Hackenberg et al. [57] predicted 97 target genes of drought responsive miRNAs in GP and identified eight targets through degradome sequencing, which were all cleaved outside of the 10^{th}-11^{th} nt site. Thus, both studies suggest the presence of non-canonical miRNA directed cleavage. Of note, both studies relied on the same degradome sequencing dataset from GP, while Ferdous et al. also observed non-canonical cleavage in an independent Pallas dataset. Moreover, in a study performed by Curaba et al. [58] 96 target genes of GP for miRNAs involved in seed development and germination were identified by degradome sequencing and only 16 targets were cleaved exclusively at the 10^{th}-11^{th} nt site, while the other targets were sporadically cleaved with an offset (24) and 56 were cleaved in majority in a non-canonical site. Finally, Deng et al. [59] identify in the barley cultivar Morex 65 target genes of 39 miRNAs, and for only 32% of the identified targets the canonical 10^{th}-11^{th} nt cleavage product was the major degradome product. Together these studies highlight the challenges in the identification of cleavage sites of sRNAs in barley and cleavage sites of tRFs in plants. The absence of canonical cleavage products for tRFs does therefore not exclude the tRF-directed cleavage of *HvBAK1*, *HvEOL1* and *HvSERK2*.

We found that 22 *Fg*-sRNAs target *HvEOL1*, a putative negative regulator of ET biosynthesis in barley. In *Arabidopsis thaliana* the EOL1 homolog *At*ETO1 acts together with *At*EOL1 and *At*ETO1-like 2 (EOL2) in directing the ubiquitination and subsequent degradation of type-2 1-aminocyclopropane-1-carboxylate synthase (ACS) proteins (e.g. ET overproducer 2 (ETO2)) [40, 60]. ET is a gaseous plant hormone that plays an important role in regulating plant growth and development, and is critical for pathogen interaction and abiotic stresses [61]. Generally, ET acts synergistically with jasmonate (JA) in the defence response against necrotrophic pathogens and this ET/JA response has antagonistic effects on salicylic acid (SA) signalling against biotrophic pathogens. Yet in low amounts JA and SA act synergistically [62, 63]. Therefore, controlling both ET biosynthesis and ET signalling is crucial for plants. Towards this, plants have evolved complex mechanisms that allow tight regulation of ET pathways e.g. at the level of (i) ET production mainly by regulating ACS gene family members, (ii) ET perception through constitutive triple response 1 (CTR1)-mediated inhibition of positive regulator ET insensitive 2 (EIN2) [64, 65], and (iii) expression of ET-responsive TFs (e.g. ET response factor 1 (ERF1)) via EBF-mediated degradation of ET insensitive 3 (EIN3) [66] (S4 Fig). According to the anticipated role of ET in the plant response to necrotrophic pathogens, such as *Fg*, targeting negative regulators of ET synthesis such as *HvEOL1* would be detrimental to *Fg* colonization. Of note, our findings are consistent with previous results demonstrating that *Fg* exploits ET signalling to enhance colonization of Arabidopsis, wheat and barley [67], supposedly through an increase in DON-induced cell death through ET. These findings further challenge the role of ET in defence against necrotrophic pathogens. Strikingly, the authors showed that in Arabidopsis ET overproducing mutants (ETO1 and ETO2) and a negative regulator of ET signalling (CTR1) are more susceptible to *Fg*, while *At* mutants in ET perception (ETR1) and signalling (EIN2 and EIN3) are resistant. These findings were confirmed by the direct application of ET during the infection of wheat and barley, which lead to increased susceptibility to *Fg*. Based on these findings, we suggest that negative regulators of ET are efficient targets for sRNA-directed manipulation of host immunity by *Fg*.

The bacterial pathogen *Pseudomonas syringae* secretes two effector molecules, AvrPto and AvrPtoB, into host plants. These effectors interact with the receptor-like kinase BRI1-associated receptor kinase 1 (BAK1), also known as SERK3, thereby preventing the recognition of

various MAMPs through the association of BAK1 with pattern recognition receptors (PRRs) such as flagellin-sensitive 2 (FLS2) and Ef-Tu receptor (EFR) [68]. We observed *FgDCL*-dependent silencing of the cereal BAK1 homologs *HvBAK1*, *HvSERK2* and *BdSERK2*. While these genes have a higher similarity to *AtSERK2* than to *AtSERK3* (*AtBAK1*), they still are among the closest homologs to *AtBAK1* found in cereals (S9 Fig). It is tempting to speculate that further experiments will uncover additional hubs that are targeted both by protein and sRNA effectors.

Conclusion

Our data show that in the necrotrophic ascomycete *Fusarium graminearum* gene silencing by RNAi shapes its ability to cause disease, which is consistent with earlier results on the significance of the RNAi machinery in *Fg* [8, 35]. Pathogenicity relies on DICER-like (DCL)-dependent sRNAs that were identified as potential candidates for fungal effectors targeting defence genes in two Poaceae hosts, barley and *Brachypodium*. We identified *Fg*-sRNAs with sequence homology to host genes that were down-regulated by *Fg* during plant colonisation, while they were expressed above their level in healthy plants after infection with a DCL dKO mutant. In PH1-*dcl1/2 vs*. PH1 the strength of target gene accumulation correlated with the abundance of the corresponding *Fg*-sRNA. Our data hint to the possibility that three DCL-dependent tRFs with sequence homology to immunity-related *Ethylene overproducer 1-like 1* (*HvEOL1)* and three Poaceae orthologues of *Arabidopsis thaliana BRI1-associated receptor kinase 1* (*HvBAK1*, *HvSERK2* and *BdSERK2*) contribute to fungal virulence via targeted gene silencing.

Experimental procedures

Plants, fungi and plant infection

Fusarium graminearum (*Fg*) strain PH1, the double knock-out (dKO) PH1-*dcl1/2* (Dr. Martin Urban, Rothamsted Research, England), strain IFA65 (IFA, Department for Agrobiotechnology, Tulln, Austria) and single mutants IFA65-*dcl1* and IFA65-*dcl2* [8] were cultured on synthetic nutrient poor agar (SNA). Preparation of fungal inoculum was performed as described [69]. *Arabidopsis thaliana* ecotype Col-0 and *Atago1-27* ([70]; Polymorphism:3510706481) were grown in 8 h photoperiod at 22˚C with 60% relative humidity in a soil—sand mixture (4:1) (Fruhstorfer Type T, Hawita, Germany). For infection, 15 rosette leaves were detached and transferred in square Petri plates containing 1% water-agar. Drop-inoculation of *At* leaves was done with 5 μl of a suspension of 5×10^4 *Fg* conidia ml^{-1} at two spots per leaf. Infection strength was recorded as infection area (size of chlorotic lesions relative to total leaf area) using the ImageJ software (https://imagej.nih.gov/ij/).

For infection of barley (*Hordeum vulgare* cv. Golden Promise, GP) and *Brachypodium distachyon* (Bd21-3), plants were grown in a 16 h photoperiod at 20˚C/18˚C day/night and 60% relative humidity in soil (Fruhstorfer Type LD80, Hawita). Ten detached second leaves were transferred into square Petri plates containing 1% water-agar. GP leaves were drop-inoculated with 3 μl of 1.5×10^5 conidia ml^{-1} conidia suspension. Bd21-3 leaves were drop-inoculated on two spots with 10 μl of 1×10^4 conidia ml^{-1} conidia suspension. Infection strength was measured with the PlantCV v2 software package (https://plantcv.danforthcenter.org/) (*Hv*) by training a machine learning algorithm to recognize necrotic lesions or by ImageJ (*Bd*). For gene expression analysis, a suspension of 5×10^4 *Fg* conidia ml^{-1} was used and leaves were either inoculated on 3 spots with 20 μl (*Hv*) or on 2 spots with 10 μl (*Bd*), respectively and experiments were evaluated 5 dpi or 4 dpi for strain PH1 on *Bd*.

Fungal transcript analysis

Gene expression analysis was performed using reverse transcription quantitative PCR (RT-qPCR). RNA extraction was performed with GENEzol reagent (Geneaid) following the manufacturer's instructions. DNA was digested with DNAse I (Thermo Scientific) according to manufacturer protocol and remaining RNA was used for cDNA synthesis using qScript™ cDNA kit (Quantabio). For RT-qPCR, 10 ng of cDNA was used as template in the QuantStudio 5 Real-Time PCR system (Applied Biosystems). Amplifications were performed with 5 μl of SYBR® green JumpStart Taq ReadyMix (Sigma-Aldrich) with 5 pmol oligonucleotides. Each sample had three technical repetitions. After an initial activation step at 95˚C for 5 min, 40 cycles (95˚C for 30 sec, 60˚C for 30 sec, 72˚C for 30 sec) were performed followed by a melt curve analysis (60˚C-95˚C, 0.075˚C/s). Ct values were determined with the QuantStudio design and analysis software supplied with the instrument. Transcript levels were determined via the $2^{-\Delta\Delta Ct}$ method [71] by normalizing the amount of target transcript to the amount of the reference transcript *Elongation factor 1-alpha* (*EF1-a*, FGSG_08811) gene (S2 Table).

Plant transcript analysis

Leaves were shock frozen at 5 dpi and RT-qPCR was performed as for fungal transcript analysis. Reference genes were *Ubiquitin-40S ribosomal protein S27a-3* (HORVU1Hr1G023660) for GP and *Ubi4* (Bradi3g04730) for Bd21-3 according to Chambers et al. [72] (S1 Table). Primers were designed using Primer3 v2.4.0 [73].

Spray application of dsRNA

Second leaves of 2 to 3-week-old GP were detached and transferred to square Petri plates containing 1% water agar. dsRNA was diluted in 500 μl water to a final concentration of 20 ng μl^{-1}. As control, Tris-EDTA (TE) buffer was diluted in 500 μl water corresponding to the amount used for dilution of the dsRNA. Typical RNA concentration after elution was 500 ng μl^{-1}, with 400 μM Tris-HCL and 40 μM EDTA in the final dilution. Each plate containing 10 detached leaves was evenly sprayed with either dsRNAs or TE buffer with 500 μl, and subsequently kept at room temperature [10]. Two days after spraying, leaves were drop-inoculated with three 20 μl drops of *Fg* suspension containing 5×10^4 conidia ml^{-1}. After inoculation, plates were closed and incubated for five days at room temperature.

Target prediction for sRNAs

RNA was purified and enriched for sRNAs from fungal axenic culture (PRJNA749737) using the mirVana miRNA Isolation Kit (Life Technologies). Indexed sRNA libraries were constructed from these sRNA fractions with the NEBNext Multiplex Small RNA Library Prep Set for Illumina (New England Biolabs) according to the manufacturer's instructions. Reads were trimmed with the cutadapt tool v2.1 [74] by removing adapters and retaining reads with a length of 21–24 nt and quality checked with the fastQC tool v0.11.9 (http://www.bioinformatics.babraham.ac.uk/projects/fastqc/). For S1 Fig reads were aligned to the *Fg* reference genome (GCF_000240135.3_ASM24013v3) with bowtie2 [75] following a sensitive alignment policy (-D 100, -R 10, -L 19). The aligned reads were assigned to the additional attribute "gene_biotype" with htseq-count [76] according to the latest assembly (ftp://ftp.ensemblgenomes.org/pub/release-44/fungi/gff3/fungi_ascomycota3_collection/fusarium_graminearum_gca_000240135). Remaining reads were collapsed with the fastx toolkit v0.0.14 [77] and reads with at least 400 reads were targeted against the IBSC_PGSB_v2 cDNA annotation with the plant miRNA target prediction algorithm TAPIR [42], following the optimized

parameters according to Srivastava et al. [39]. The results of the target prediction were further analysed with RStudio [78] and the package biomaRt [79] to find targets associated with stress and immunity associated Gene ontology (GO) terms in the database "plants_mart" from plants.ensembl.org hosted by the EBI (European Bioinformatics Institute) and the Wellcome Trust Sanger Institute. The same method was used for the identification of target genes in *B. distachyon* (GCA_000005505.4) and *A. thaliana* (Araport11).

Stemloop-RT-qPCR of sRNAs

RNA was extracted and genomic DNA was digested as described for the transcript analyses. The sequences of sRNAs found in axenic fungal culture were used to design specific stem loop (SL) primers matching the sRNA over 6 nt at the 3'end. For the primer design, the tool of Adhikari et al. [80] was used. SL-primers were diluted to 10 pM and folded in a cycler (95˚C for 15 min, 90˚C 5 min, 85˚C 5 min, 80˚C 5 min, 75˚C 1 h, 68˚C 1 h, 65˚C 1 h, 62˚C 1 h, 60˚C 3 h). These primers were used for cDNA synthesis (Thermo Scientific RevertAid RT Reverse Transcription Kit) according to manufacturer's instruction with an annealing step at 16˚C instead of 25˚C and were used in multiplex to target respective fungal sRNAs and barley miRNAs *Hvu*-mir159 and *Hvu*-mir168 as references. To obtain amplification efficiencies, a mix from all RNAs was diluted in a four step dilution series with a factor of ten and reverse transcribed. Reactions were set up with the highest concentration of 15 ng μl^{-1} and the lowest of 15 pg μl^{-1} cDNA. All sRNA amplifications showed an efficiency of 80–82% and an R^2 between 1 and 0.997 except for Fg-sRNA-6717 with an efficiency of 66.4%. For RT-qPCR, 1.5 μl of 3 ng μl^{-1} cDNA was used as template in the QuantStudio 5 Real-Time PCR system (Applied Biosystems). Amplifications were performed with 5 μl of SYBR® green JumpStart Taq ReadyMix (Sigma-Aldrich) with 1.5 pmol or 3 pmol oligonucleotides. Each sample had three technical repetitions. As forward primer the unused nucleotides of the remaining sequence of the sRNA were used, which were extended to achieve optimal melting temperature, and as reverse primer the universal stem loop primer developed by Chen et al. [41] was used. Relative abundance of the sRNAs was calculated with the ΔΔct-method with incorporation of amplification efficiencies. sRNAs were normalized against the reference miRNAs Hvu-mir-159a and 168-5p and after this against the fungal biomass measured as *EF1-α* against *HvUBQ* (*HORVU1Hr1G023660*).

Statistics

To assess the differential expression of genes via RT-qPCRs the Δct values were compared via a one or two sided paired Students *t*-test. Disease symptoms were either compared via Students *t*-test if the data showed a normal distribution in Shapiro-Wilk test or via a Wilcoxon rank sum test.

RLM-RACE

RNA from GP barley infected with *Fg*-IFA65 at 5 dpi and an uninfected control was extracted with the Isolate II plant miRNA kit (Bioline). 1 μg of RNA (>200 nt) of infected, uninfected and a mix of both samples for a–RT-control were assembled. 1 μl of the 5'RACE Adapter [0.3 μg/μl], 1 μl of the 10x Reaction Buffer, 1 μl of 1mg/μl BSA, 0.5 μl of T4 RNA Ligase [10U/μl] (Thermo Scientific) and DEPC-treated water up to 10 μl were prepared and incubated at 37˚C for 60 min. Subsequently, the whole reaction was used for reverse transcription (RevertAid Reverse Transcriptase, Thermo Scientific). 10 μl ligation reaction, 1 μl Random Hexamer [100pmol/μl], 4 μl 5x Reaction Buffer, 0.5 μl RiboLock RNase Inhibitor (Thermo Scientific), 2 μl dNTP Mix [10 mM] and 1 μl RevertAid Reverse Transcriptase (or water (–RT control))

and 1.5 μl water were mixed and run for 10 min at 25˚C, 60 min at 42˚C and 10 min at 70˚C. Then, a nested hot-start touch-down PCR for each target gene was performed. The primer sequences for the outer (first) and inner (second) PCR are shown in S1 Table. 5 μl of 10x Buffer B, 1 μl of a dNTP Mix [10 mM], 2 μl $MgCl_2$ [25 mM], 1μl Adapter specific Primer [10 pmol μl^{-1}] and 1 μl gene specific primer (GSP) [10 pmol μl^{-1}], 0.6 μl DCS DNA Polymerase (DNA Cloning Service) [5 U/μl] and 2 μl cDNA or outer PCR reaction and 37.4 μl water were mixed and run at 95˚C for 5 min, (95˚for 30 s, 68˚C-0.5˚C/cycle for 30 s, 72˚C for 30 s)*15, (95˚C for 30 s, 60˚C for 30 s, 72˚C for 30 s)*18 and 72˚C for 5 min. PCR products were evaluated in a 1.5% agarose gel and bands of the expected size, which were present in the infected but not uninfected samples, were excised. Products were cleaned with the Wizard SV Gel and PCR Clean-Up System (Promega) and cloned with the pGEM-T easy Vector Systems (Promega). For each band, five clones were picked for sequencing. Plasmids from O/N cultures were extracted with the Monarch Plasmid Miniprep Kit (New England Biolabs) and sent for sequencing to LGC genomics.

Analysis of target genes and targeting sRNAs

After the initial target prediction an additional target prediction for the newly released cultivar specific genome (GCA_902500625) of barley cv. Golden Promise (GP) was conducted. Adapters were removed and reads were collapsed as described before for the target prediction. All sRNA sequences were read with SeqinR v3.6–1 [81] and stored in a list of SeqFastadna objects. To identify the homologous genes to the already identified targets in GP, the cDNA library was blasted with the command-line blast application (Nucleotide-Nucleotide BLAST 2.6.0+) [82] against the identified target sequences from the IBSC_PGSB_v2 cDNA library with percent identity of 90 and a query coverage of 55% as cut-off values. All sRNAs with at least two reads were written to a file in chunks of 2000 each and ran against each individual target gene with TAPIR via the system2 function in R [83] in the RStudio software. Results were collected, stored in a data.frame, and further analysed with R. sRNAs identified to target a gene of interest (GOI) were written to a fasta file with SeqinR and blasted against the rRNAs from the assemblies GCA_900044135.1 (*Fg*-PH1), GCA_000240135.3 (*Fg*-PH1) and the *Fusarium* rRNAs from the RNAcentral fungal ncRNA dataset (ftp://ftp.ebi.ac.uk/pub/databases/RNAcentral/current_release/sequences/by-database/ensembl_fungi.fasta (12/Sep/2020)) with the options wordsize = 4, perc_identity = 95, qcov_hsp_perc = 95. All sRNAs matching rRNAs were removed. Thereafter, sRNAs were compared to the *Fg* assemblies GCA_900044135.1 (*Fg*-PH1) and GCA_000240135.3 (*Fg*-PH1) with the same blast strategy and only perfectly matching sRNAs were retained.

To derive the relative expression of a GOI between two samples the following formula is used.

$$Relativeexpression_{GOI} = 2^{-\Delta\Delta ct_{GOI}}$$

We further defined the ΔΔΔct value as the difference between the ΔΔct values for a GOI in PH1 and PH1-*dcl1/2*-infected samples.

$$\Delta\Delta\Delta\mathrm{ct} = \Delta\Delta ct_{PH1-dcl1/2} - \Delta\Delta ct_{PH1}$$

This enables the calculation of the re-accumulation between the two samples as follows.

$$DCL-dependent\ \ resurgence\ \ factor = \frac{Relativeexpression_{PH1-dcl1/2}}{Relativeexpression_{PH1}} = 2^{-\Delta\Delta\Delta ct_{GOI}}$$

The sum of all reads and the corresponding ΔΔΔct-value were plotted with ggplot2 [84] and

a linear regression was added to the plot. To allow a log2-transformation of the plots genes with zero targeting reads were set to one targeting read. The plots were arranged using ggpubr v.0.4.0 [85].

GO enrichment analysis

Gene ontology (GO) enrichment analysis was performed via the AgriGO v.2.0 analysis toolkit [86] with the standard parameters singular enrichment analysis (SEA).

Phylogenetic analysis of SERK homologs

Homologs of *HvBAK1* and *HvSERK2* were searched in *At*, *Hv* and *Bd* with biomaRt v.2.40.5 [79] and downloaded from the EMBL's European Bioinformatics Institute plants genome page (plants.ensembl.org) in the plants_mart dataset hvulgare_eg_gene (Ensembl Plants Genes v. 50). For these homologs the CDS of all homologs within the respective datasets athaliana_eg_gene, hvulgare_eg_gene and bdistachyon_eg_gene were downloaded. The CDS were subsequently aligned with the muscle algorithm in MEGA7 [87] and a phylogenetic tree was constructed via a bootstrap method with 200 iterations.

Supporting information

S1 Fig. Feature mapping of *Fg*-sRNAs with a read length of 21–24 nt. Reads were trimmed as described earlier and aligned to the PH1 reference genome (GCF_000240135.3_ASM24013v3) with bowtie2 [75].
(TIF)

S2 Fig. GO-enrichment analysis of all potential targets of *Fg*-sRNAs with more than 400 reads. The plot shows all significantly enriched GO-terms in the target gene set for (A) molecular function and (B) biological process. The analysis was done using agriGo v2.0. Each box contains information regarding one term. GO: indicates the GO accession, in brackets the p-value is stated (Fisher; Yekutieli (FDR)). After the bracket the GO-term description is written followed by the number of genes associated with said term 1. in the gene set and 2. In the background.
(TIF)

S3 Fig. Alignment of AtETO1 and HvEOL1. Identical amino acids are marked blue and similar amino acids are marked red. The alignment and visualization was done with the msa package for R [88].
(TIF)

S4 Fig. Regulation of ET synthesis in At. *At*ETO1 negatively regulates ethylene **(ET)** synthesis in *At*. *At*ETO1 acts together with *At*EOL1 and *At*ETO1-like 2 (EOL2) in directing the ubiquitination and subsequent degradation of type-2 1-aminocyclopropane-1-carboxylate synthase (ACS) proteins (e.g. ET overproducer 2 (ETO2)), which produce the direct precursor of ET.
(TIF)

S5 Fig. Sequences of dsRNA-dcl1/2. Coding Sequences (CDS) of the respective *FgDCL* genes with the sequences comprising the dsRNAs marked in red. A. FgDCL1-FGSG_09025 (912 nt long dsRNA-FgDCL1). B. FgDCL2-FGSG_04408 (870 nt long dsRNA-FgDCL2).
(TIF)

S6 Fig. Position and read count of all tRFs from *Fg*-tRNA-Gly(GCC). Alignment position of all *Fg*-sRNAs from axenic culture with more than 50 reads perfectly matching the *Fg*-tRNA-Gly(GCC)-9 gene (Fusarium_graminearum_CS3005-tRNA-Gly-GCC-1-9) colored by read count.
(TIF)

S7 Fig. Abundance of unique *Fg*-sRNAs in axenic culture of IFA65. A: Histogram of the read count of every unique sRNA. The plot is truncated to make abundances recognizable. Most sRNAs have very low read counts and very few sRNAs have more reads than 3,000. Maximum read count per sRNA is 42,866. B: Violin plot of log2-transformed reads counts untruncated.
(TIF)

S8 Fig. Origin of tRFs in *Fg*-tRNA-Gly(GCC). The centroid secondary structure of the *Fg*-tRNA-Gly(GCC) generated on the RNAfold web server (http://rna.tbi.univie.ac.at/cgi-bin/RNAWebSuite/RNAfold.cgi) with the origin and alignment of *Fg*-sRNA-321, *Fg*-sRNA-1921 and *Fg*-sRNA-6717. The colors of bases indicate the base pair probabilities.
(TIF)

S9 Fig. Molecular Phylogenetic analysis by maximum likelihood method. The evolutionary history was inferred by using the Maximum Likelihood method based on the General Time Reversible model [89]. The tree with the highest log likelihood (-25430.37) is shown. Initial tree(s) for the heuristic search were obtained automatically by applying Neighbor-Join and BioNJ algorithms to a matrix of pairwise distances estimated using the Maximum Composite Likelihood (MCL) approach, and then selecting the topology with superior log likelihood value. The tree is drawn to scale, with branch lengths measured in the number of substitutions per site. The analysis involved 77 nucleotide sequences. Codon positions included were 1st +2nd+3rd. There were a total of 2427 positions in the final dataset. Evolutionary analyses were conducted in MEGA7 [87].
(TIF)

S10 Fig. Unedited gel images from Fig 6.
(PDF)

S1 Table. Primer sequences.
(DOCX)

S2 Table. Target prediction results. Results of the target prediction with the TAPIR algorithm for all *Fg*-sRNAs with more than 400 reads.
(XLSX)

Acknowledgments

We thank the Salk Institute Genomic Analysis Laboratory for providing the sequence-indexed Arabidopsis TDNA insertion mutants.

Author Contributions

Conceptualization: Bernhard Timo Werner, Aline Koch, Karl-Heinz Kogel.

Data curation: Bernhard Timo Werner, Aline Koch, Lukas Jelonek.

Formal analysis: Bernhard Timo Werner, Ena Šečić, Jonas Engelhardt, Lukas Jelonek.

Funding acquisition: Aline Koch, Jens Steinbrenner, Karl-Heinz Kogel.

Investigation: Aline Koch, Ena Šečić, Karl-Heinz Kogel.

Methodology: Bernhard Timo Werner, Aline Koch, Ena Šečić, Jonas Engelhardt, Jens Steinbrenner.

Project administration: Aline Koch, Jens Steinbrenner, Karl-Heinz Kogel.

Resources: Bernhard Timo Werner.

Software: Bernhard Timo Werner, Ena Šečić, Jonas Engelhardt, Lukas Jelonek.

Supervision: Aline Koch, Jens Steinbrenner, Karl-Heinz Kogel.

Validation: Bernhard Timo Werner.

Visualization: Bernhard Timo Werner.

Writing – original draft: Bernhard Timo Werner, Aline Koch, Karl-Heinz Kogel.

Writing – review & editing: Bernhard Timo Werner, Aline Koch, Ena Šečić, Lukas Jelonek, Jens Steinbrenner, Karl-Heinz Kogel.

References

1. Koch A., & Kogel K. H. (2014). New wind in the sails: improving the agronomic value of crop plants through RNA i-mediated gene silencing. *Plant biotechnology journal*, 12(7), 821–831. https://doi.org/10.1111/pbi.12226 PMID: 25040343
2. Guo Q., Liu Q., Smith N.A., Liang G., & Wang M.B. (2016). RNA Silencing in plants: mechanisms, technologies and applications in horticultural crops. *Current Genomics*, 17, 476–489. https://doi.org/10.2174/1389202917666160520103117 PMID: 28217004
3. Liu S., Jaouannet M., Dempsey D. M. A., Imani J., Coustau C., & Kogel K. H. (2020). RNA-based technologies for insect control in plant production. *Biotechnology advances*, 39, 107463. https://doi.org/10.1016/j.biotechadv.2019.107463 PMID: 31678220
4. Šečić E and Kogel KH (2021). Requirements for fungal uptake of dsRNA and gene silencing in RNAi-based crop protection strategies. *Current Opinion in Biotechnology*, COBIOT-D-21-00048. https://doi.org/10.1016/j.copbio.2021.04.001 PMID: 34000482
5. Koch A., & Wassenegger M. (2021). Host-induced gene silencing–mechanisms and applications. *New Phytologist*, 231(1), 54–59. https://doi.org/10.1111/nph.17364 PMID: 33774815
6. Rosa C., Kuo Y. W., Wuriyanghan H., & Falk B. W. (2018). RNA interference mechanisms and applications in plant pathology. *Annual review of phytopathology*, 56, 581–610. https://doi.org/10.1146/annurev-phyto-080417-050044 PMID: 29979927
7. Cai Q., He B., Kogel K. H., & Jin H. (2018). Cross-kingdom RNA trafficking and environmental RNAi—nature's blueprint for modern crop protection strategies. *Current opinion in microbiology*, 46, 58–64. https://doi.org/10.1016/j.mib.2018.02.003 PMID: 29549797
8. Gaffar F. Y., Imani J., Karlovsky P., Koch A., & Kogel K.-H. (2019). Different components of the RNA interference machinery are required for conidiation, ascosporogenesis, virulence, deoxynivalenol production, and fungal inhibition by exogenous double-stranded RNA in the Head Blight pathogen *Fusarium graminearum*. *Frontiers in Microbiology*, 10, 1662. https://doi.org/10.3389/fmicb.2019.01662 PMID: 31616385
9. Niehl A., & Heinlein M. (2019). Perception of double-stranded RNA in plant antiviral immunity. *Molecular plant pathology*, 20(9), 1203–1210. https://doi.org/10.1111/mpp.12798 PMID: 30942534
10. Koch A., Biedenkopf D., Furch A., Weber L., Rossbach O., Abdellatef E., et al. (2016). An RNAi-based control of *Fusarium graminearum* infections through spraying of long dsRNAs involves a plant passage and is controlled by the fungal silencing machinery. *PLoS pathogens*, 12(10), e1005901. https://doi.org/10.1371/journal.ppat.1005901 PMID: 27737019
11. Wang M., Weiberg A., Lin F.-M., Thomma B. P. H. J., Huang H.D., & Jin H. (2016). Bidirectional cross-kingdom RNAi and fungal uptake of external RNAs confer plant protection. *Nature Plants*, 2, 16151. https://doi.org/10.1038/nplants.2016.151 PMID: 27643635
12. Konakalla N. C., Kaldis A., Berbati M., Masarapu H., & Voloudakis A. E. (2016). Exogenous application of double-stranded RNA molecules from TMV p126 and CP genes confers resistance against

TMV in tobacco. *Planta*, 244(4), 961–969. https://doi.org/10.1007/s00425-016-2567-6 PMID: 27456838

13. Mitter N., Worrall E. A., Robinson K. E., Li P., Jain R. G., Taochy C., et al. (2017). Clay nanosheets for topical delivery of RNAi for sustained protection against plant viruses. *Nature plants*, 3(2), 1–10. https://doi.org/10.1038/nplants.2016.207 PMID: 28067898
14. Kaldis A., Berbati M., Melita O., Reppa C., Holeva M., Otten P., et al. (2018). Exogenously applied dsRNA molecules deriving from the Zucchini yellow mosaic virus (ZYMV) genome move systemically and protect cucurbits against ZYMV. *Molecular plant pathology*, 19(4), 883–895. https://doi.org/10.1111/mpp.12572 PMID: 28621835
15. McLoughlin A. G., Wytinck N., Walker P. L., Girard I. J., Rashid K. Y., de Kievit T., et al. (2018). Identification and application of exogenous dsRNA confers plant protection against Sclerotinia sclerotiorum and Botrytis cinerea. *Scientific Reports*, 8(1), 1–14. https://doi.org/10.1038/s41598-017-17765-5 PMID: 29311619
16. Sang H., & Kim J. I. (2020). Advanced strategies to control plant pathogenic fungi by host-induced gene silencing (HIGS) and spray-induced gene silencing (SIGS). *Plant Biotechnology Reports*, 14(1), 1–8.
17. Head G. P., Carroll M. W., Evans S. P., Rule D. M., Willse A. R., Clark T. L., et al. (2017). Evaluation of SmartStax and SmartStax PRO maize against western corn rootworm and northern corn rootworm: efficacy and resistance management. *Pest management science*, 73(9), 1883–1899. https://doi.org/10.1002/ps.4554 PMID: 28195683
18. Niehl A., Soininen M., Poranen M. M., & Heinlein M. (2018). Synthetic biology approach for plant protection using ds RNA. *Plant biotechnology journal*, 16(9), 1679–1687.
19. Weiberg A., Wang M., Lin F. M., Zhao H., Zhang Z., Kaloshian I., et al. (2013). Fungal small RNAs suppress plant immunity by hijacking host RNA interference pathways. *Science*, 342(6154), 118–123. https://doi.org/10.1126/science.1239705 PMID: 24092744
20. Cai Q., Qiao L., Wang M., He B., Lin F. M., Palmquist J., et al. (2018). Plants send small RNAs in extracellular vesicles to fungal pathogen to silence virulence genes. *Science*, 360(6393), 1126–1129. https://doi.org/10.1126/science.aar4142 PMID: 29773668
21. Wang M., Weiberg A., Dellota E. Jr, Yamane D, & Jin H. (2017). Botrytis small RNA Bc-siR37 suppresses plant defense genes by cross-kingdom RNAi. *RNA Biology*, 14, 421–428. https://doi.org/10.1080/15476286.2017.1291112 PMID: 28267415
22. Dunker F., Trutzenberg A., Rothenpieler J. S., Kuhn S., Pröls R., Schreiber T., et al. (2020). Oomycete small RNAs bind to the plant RNA-induced silencing complex for virulence. *Elife*, 9, e56096. https://doi.org/10.7554/eLife.56096 PMID: 32441255
23. Wang B., Sun Y.F., Song N., Zhao M.X., Liu R., Feng H., et al. (2017). *Puccinia striiformis f. sp tritici* microRNA-like RNA 1 (Pst-milR1), an important pathogenicity factor of Pst, impairs wheat resistance to Pst by suppressing the wheat pathogenesis-related 2 gene. *New Phytologist*, 215, 338–350.
24. Dubey H., Kiran K., Jaswal R., Jain P., Kayastha A. M., Bhardwaj S. C., et al. (2019). Discovery and profiling of small RNAs from Puccinia triticina by deep sequencing and identification of their potential targets in wheat. *Functional & integrative genomics*, 19(3), 391–407. https://doi.org/10.1007/s10142-018-00652-1 PMID: 30618015
25. Mueth N. A., Ramachandran S. R., & Hulbert S. H. (2015). Small RNAs from the wheat stripe rust fungus (Puccinia striiformis f. sp. tritici). *Bmc Genomics*, 16(1), 1–16.
26. Reinhart B. J., Weinstein E. G., Rhoades M. W., Bartel B., & Bartel D. P. (2002). MicroRNAs in plants. *Genes & development*, 16(13), 1616–1626. https://doi.org/10.1101/gad.1004402 PMID: 12101121
27. Ren B., Wang X., Duan J., & Ma J. (2019). Rhizobial tRNA-derived small RNAs are signal molecules regulating plant nodulation. *Science*, 365(6456), 919–922. https://doi.org/10.1126/science.aav8907 PMID: 31346137
28. Jones-Rhoades M. W. (2012). Conservation and divergence in plant microRNAs. *Plant molecular biology*, 80(1), 3–16. https://doi.org/10.1007/s11103-011-9829-2 PMID: 21996939
29. Garcia-Silva M. R., Cabrera-Cabrera F., Cura das Neves R. F., Souto-Padrón T., de Souza W., & Cayota A. (2014). Gene expression changes induced by *Trypanosoma cruzi* shed microvesicles in mammalian host cells: relevance of trna-derived halves. *BioMed Research International*, 2014, 1–11. https://doi.org/10.1155/2014/305239 PMID: 24812611
30. Dean R., Van Kan J. A., Pretorius Z. A., Hammond-Kosack K. E., Di Pietro A., Spanu P. D., et al. (2012). The Top 10 fungal pathogens in molecular plant pathology. *Molecular plant pathology*, 13(4), 414–430. https://doi.org/10.1111/j.1364-3703.2011.00783.x PMID: 22471698
31. Desjardins A. E., Hohn T. M., & McCORMICK S. P. (1993). Trichothecene biosynthesis in *Fusarium* species: chemistry, genetics, and significance. *Microbiology and Molecular Biology Reviews*, 57(3), 595–604.

32. Jansen C., Von Wettstein D., Schäfer W., Kogel K. H., Felk A., & Maier F. J. (2005). Infection patterns in barley and wheat spikes inoculated with wild-type and trichodiene synthase gene disrupted *Fusarium graminearum*. *Proceedings of the National Academy of Sciences*, 102(46), 16892–16897. https://doi.org/10.1073/pnas.0508467102 PMID: 16263921

33. Ilgen P., Hadeler B., Maier F. J., & Schäfer W. (2009). Developing kernel and rachis node induce the trichothecene pathway of *Fusarium graminearum* during wheat head infection. *Molecular plant-microbe interactions*, 22(8), 899–908. https://doi.org/10.1094/MPMI-22-8-0899 PMID: 19589066

34. Kim H. K., Jo S. M., Kim G. Y., Kim D. W., Kim Y. K., & Yun S. H. (2015). A large-scale functional analysis of putative target genes of mating-type loci provides insight into the regulation of sexual development of the cereal pathogen *Fusarium graminearum*. *PLoS Genet*, 11(9), e1005486. https://doi.org/10.1371/journal.pgen.1005486 PMID: 26334536

35. Son H, Park AR, Lim JY, Shin C, Lee Y-W (2017) Genome-wide exonic small interference RNA-mediated gene silencing regulates sexual reproduction in the homothallic fungus *Fusarium graminearum*. PLoS Genet 13(2): e1006595. https://doi.org/10.1371/journal.pgen.1006595 PMID: 28146558

36. Ji H., Mao H., Li S., Feng T., Zhang Z., Cheng L., et al. (2021). *Fol*-milR1, a pathogenicity factor of *Fusarium oxysporum*, confers tomato wilt disease resistance by impairing host immune responses. *New Phytologist*, nph.17436. https://doi.org/10.1111/nph.17436 PMID: 33960431

37. Jian J., & Liang X. (2019). One small RNA of *Fusarium graminearum* targets and silences CEBiP gene in common wheat. *Microorganisms*, 7(10), 425. https://doi.org/10.3390/microorganisms7100425 PMID: 31600909

38. Mascher M., Gundlach H., Himmelbach A., Beier S., Twardziok S. O., Wicker T., et al. (2017). A chromosome conformation capture ordered sequence of the barley genome. *Nature*, 544(7651), 427–433. https://doi.org/10.1038/nature22043 PMID: 28447635

39. Srivastava P. K., Moturu T. R., Pandey P., Baldwin I. T., & Pandey S. P. (2014). A comparison of performance of plant miRNA target prediction tools and the characterization of features for genome-wide target prediction. *BMC genomics*, 15(1), 1–15. https://doi.org/10.1186/1471-2164-15-348 PMID: 24885295

40. Christians M. J., Gingerich D. J., Hansen M., Binder B. M., Kieber J. J., & Vierstra R. D. (2009). The BTB ubiquitin ligases ETO1, EOL1 and EOL2 act collectively to regulate ethylene biosynthesis in Arabidopsis by controlling type-2 ACC synthase levels. *The Plant Journal*, 57(2), 332–345. https://doi.org/10.1111/j.1365-313X.2008.03693.x PMID: 18808454

41. Chen C., Ridzon D. A., Broomer A. J., Zhou Z., Lee D. H., Nguyen J. T., et al. (2005). Real-time quantification of microRNAs by stem–loop RT–PCR. *Nucleic acids research*, 33(20), e179–e179. https://doi.org/10.1093/nar/gni178 PMID: 16314309

42. Bonnet E., He Y., Billiau K., & Van de Peer Y. (2010). TAPIR, a web server for the prediction of plant microRNA targets, including target mimics. *Bioinformatics*, 26(12), 1566–1568. https://doi.org/10.1093/bioinformatics/btq233 PMID: 20430753

43. Mallory A. C., Reinhart B. J., Jones-Rhoades M. W., Tang G., Zamore P. D., Barton M. K., et al. (2004). MicroRNA control of PHABULOSA in leaf development: importance of pairing to the microRNA 5′ region. *The EMBO journal*, 23(16), 3356–3364. https://doi.org/10.1038/sj.emboj.7600340 PMID: 15282547

44. Werner B. T., Gaffar F. Y., Schuemann J., Biedenkopf D., & Koch A. M. (2020). RNA-spray-mediated silencing of *Fusarium graminearum* AGO and DCL genes improve barley disease resistance. *Frontiers in Plant Science*, 11, 476. https://doi.org/10.3389/fpls.2020.00476 PMID: 32411160

45. Lax C., Tahiri G., Patiño-Medina J. A., Cánovas-Márquez J. T., Pérez-Ruiz J. A., Osorio-Concepción M., et al. (2020). The Evolutionary Significance of RNAi in the Fungal Kingdom. *International Journal of Molecular Sciences*, 21(24), 9348. https://doi.org/10.3390/ijms21249348 PMID: 33302447

46. Zanini S., Šečić E., Busche T., Galli M., Zheng Y., Kalinowski J., et al. (2021). Comparative Analysis of Transcriptome and sRNAs Expression Patterns in the *Brachypodium distachyon—Magnaporthe oryzae* Pathosystems. *International Journal of Molecular Sciences*, 22(2), 650. https://doi.org/10.3390/ijms22020650 PMID: 33440747

47. Lee Marzano S. Y., Neupane A., Mochama P., Feng C., & Saleem H. (2019). Roles of argonautes and dicers on Sclerotinia sclerotiorum antiviral RNA silencing. *Frontiers in Plant Science*, 10, 976. https://doi.org/10.3389/fpls.2019.00976 PMID: 31440265

48. Åsman A. K., Vetukuri R. R., Jahan S. N., Fogelqvist J., Corcoran P., Avrova A. O., et al. (2014). Fragmentation of tRNA in Phytophthora infestans asexual life cycle stages and during host plant infection. *BMC microbiology*, 14(1), 308. https://doi.org/10.1186/s12866-014-0308-1 PMID: 25492044

49. Streit R. S. A., Ferrareze P. A. G., Vainstein M. H., & Staats C. C. (2021). Analysis of tRNA-derived RNA fragments (tRFs) in *Cryptococcus* spp.: RNAi-independent generation and possible compensatory

effects in a RNAi-deficient genotype. *Fungal Biology*, 125(5), 389–399. https://doi.org/10.1016/j.funbio.2020.12.003 PMID: 33910680

50. Kumar P., Kuscu C., & Dutta A. (2016). Biogenesis and function of transfer RNA-related fragments (tRFs). *Trends in biochemical sciences*, 41(8), 679–689. https://doi.org/10.1016/j.tibs.2016.05.004 PMID: 27263052

51. Li N., Shan N., Lu L., & Wang Z. (2021). tRFtarget: a database for transfer RNA-derived fragment targets. *Nucleic Acids Research*, 49(D1), D254–D260. https://doi.org/10.1093/nar/gkaa831 PMID: 33035346

52. Zuo Y., Zhu L., Guo Z., Liu W., Zhang J., Zeng Z., et al. (2021). tsRBase: a comprehensive database for expression and function of tsRNAs in multiple species. *Nucleic Acids Research*, 49(D1), D1038–D1045. https://doi.org/10.1093/nar/gkaa888 PMID: 33068436

53. Wang Q., Li T., Xu K., Zhang W., Wang X., Quan J., et al. (2016b). The tRNA-derived small RNAs regulate gene expression through triggering sequence-specific degradation of target transcripts in the oomycete pathogen Phytophthora sojae. *Frontiers in plant science*, 7, 1938.

54. Martinez G., Choudury S. G., & Slotkin R. K. (2017). tRNA-derived small RNAs target transposable element transcripts. *Nucleic acids research*, 45(9), 5142–5152. https://doi.org/10.1093/nar/gkx103 PMID: 28335016

55. Asha S., & Soniya E. V. (2016). Transfer RNA derived small RNAs targeting defense responsive genes are induced during Phytophthora capsici infection in black pepper (Piper nigrum L.). *Frontiers in plant science*, 7, 767. https://doi.org/10.3389/fpls.2016.00767 PMID: 27313593

56. Ferdous J., Sanchez-Ferrero J. C., Langridge P., Milne L., Chowdhury J., Brien C., et al. (2017). Differential expression of microRNAs and potential targets under drought stress in barley. *Plant, cell & environment*, 40(1), 11–24. https://doi.org/10.1111/pce.12764 PMID: 27155357

57. Hackenberg M., Gustafson P., Langridge P., & Shi B. J. (2015). Differential expression of micro RNA s and other small RNA s in barley between water and drought conditions. *Plant biotechnology journal*, 13(1), 2–13. https://doi.org/10.1111/pbi.12220 PMID: 24975557

58. Curaba J., Spriggs A., Taylor J., Li Z., & Helliwell C. (2012). miRNA regulation in the early development of barley seed. *BMC plant biology*, 12(1), 1–16. https://doi.org/10.1186/1471-2229-12-120 PMID: 22838835

59. Deng P., Wang L., Cui L., Feng K., Liu F., Du X., et al. (2015). Global identification of microRNAs and their targets in barley under salinity stress. *PLoS One*, 10(9), e0137990. https://doi.org/10.1371/journal.pone.0137990 PMID: 26372557

60. Yoshida H., Wang K.L., Chang C.M., Mori K., Uchida E., Ecker J.R. (2006). The ACC synthase TOE sequence is required for interaction with ETO1 family proteins and destabilization of target proteins. Plant Mol Biol. 62(3):427–37. https://doi.org/10.1007/s11103-006-9029-7 PMID: 16897471

61. Abeles F. B., Morgan P. W., & Saltveit M. E. (1992). CHAPTER 5—Roles and Physiological Effects of Ethylene in Plant Physiology: Dormancy, Growth, and Development. In *Ethylene in Plant Biology* (2nd ed., pp. 120–181)., Academic Press.

62. Glazebrook J. (2005). Contrasting mechanisms of defense against biotrophic and necrotrophic pathogens. *Annu. Rev. Phytopathol.*, 43, 205–227. https://doi.org/10.1146/annurev.phyto.43.040204.135923 PMID: 16078883

63. Li N., Han X., Feng D., Yuan D., & Huang L. J. (2019). Signaling crosstalk between salicylic acid and ethylene/jasmonate in plant defense: do we understand what they are whispering?. *International Journal of Molecular Sciences*, 20(3), 671. https://doi.org/10.3390/ijms20030671 PMID: 30720746

64. Kieber J. J., Rothenberg M., Roman G., Feldmann K. A., & Ecker J. R. (1993). CTR1, a negative regulator of the ethylene response pathway in Arabidopsis, encodes a member of the raf family of protein kinases. *Cell*, 72(3), 427–441. https://doi.org/10.1016/0092-8674(93)90119-b PMID: 8431946

65. Alonso J. M., Hirayama T., Roman G., Nourizadeh S., & Ecker J. R. (1999). EIN2, a bifunctional transducer of ethylene and stress responses in Arabidopsis. *Science*, 284(5423), 2148–2152. https://doi.org/10.1126/science.284.5423.2148 PMID: 10381874

66. Potuschak T., Lechner E., Parmentier Y., Yanagisawa S., Grava S., Koncz C., et al. (2003). EIN3-dependent regulation of plant ethylene hormone signaling by two Arabidopsis F box proteins: EBF1 and EBF2. *Cell*, 115(6), 679–689. https://doi.org/10.1016/s0092-8674(03)00968-1 PMID: 14675533

67. Chen X., Steed A., Travella S., Keller B., & Nicholson P. (2009). *Fusarium graminearum* exploits ethylene signalling to colonize dicotyledonous and monocotyledonous plants. *New Phytologist*, 182(4), 975–983. https://doi.org/10.1111/j.1469-8137.2009.02821.x PMID: 19383094

68. Shan L., He P., Li J., Heese A., Peck S. C., Nürnberger T., et al. (2008). Bacterial effectors target the common signaling partner BAK1 to disrupt multiple MAMP receptor-signaling complexes and impede

plant immunity. *Cell host & microbe*, 4(1), 17–27. https://doi.org/10.1016/j.chom.2008.05.017 PMID: 18621007

69. Koch A., Kumar N., Weber L., Keller H., Imani J., & Kogel K. H. (2013). Host-induced gene silencing of cytochrome P450 lanosterol C14α-demethylase–encoding genes confers strong resistance to *Fusarium* species. *Proceedings of the National Academy of Sciences*, 110(48), 19324–19329. https://doi.org/10.1073/pnas.1306373110 PMID: 24218613

70. Morel J. B., Godon C., Mourrain P., Béclin C., Boutet S., Feuerbach F., et al. (2002). Fertile hypomorphic ARGONAUTE (ago1) mutants impaired in post-transcriptional gene silencing and virus resistance. *The Plant Cell*, 14(3), 629–639. https://doi.org/10.1105/tpc.010358 PMID: 11910010

71. Livak K. J., & Schmittgen T. D. (2001). Analysis of relative gene expression data using real-time quantitative PCR and the 2− ΔΔCT method. *methods*, 25(4), 402–408. https://doi.org/10.1006/meth.2001.1262 PMID: 11846609

72. Chambers J. P., Behpouri A., Bird A., & Ng C. K. (2012). Evaluation of the use of the Polyubiquitin Genes, Ubi4 and Ubi10 as reference genes for expression studies in *Brachypodium distachyon*. *PLoS One*, 7(11), e49372. https://doi.org/10.1371/journal.pone.0049372 PMID: 23166649

73. Untergasser A., Cutcutache I., Koressaar T., Ye J., Faircloth B. C., Remm M., et al. (2012). Primer3—new capabilities and interfaces. *Nucleic acids research*, 40(15), e115–e115. https://doi.org/10.1093/nar/gks596 PMID: 22730293

74. Martin M. (2011). Cutadapt removes adapter sequences from high-throughput sequencing reads. *EMBnet. journal*, 17(1), 10–12.

75. Langmead B., & Salzberg S. L. (2012). Fast gapped-read alignment with Bowtie 2. *Nature methods*, 9(4), 357. https://doi.org/10.1038/nmeth.1923 PMID: 22388286

76. Anders S., Pyl P. T., & Huber W. (2015). HTSeq—a Python framework to work with high-throughput sequencing data. *Bioinformatics*, 31(2), 166–169. https://doi.org/10.1093/bioinformatics/btu638 PMID: 25260700

77. Hannon, G. "Fastx-toolkit." FASTQ/A Short-reads Preprocessing Tools (2010)

78. RStudio Team (2016). RStudio: Integrated Development for R. RStudioInc., Boston, MA URL http://www.rstudio.com/.

79. Durinck S., Moreau Y., Kasprzyk A., Davis S., De Moor B., Brazma A., et al. (2005). BioMart and Bioconductor: a powerful link between biological databases and microarray data analysis. *Bioinformatics*, 21(16), 3439–3440. https://doi.org/10.1093/bioinformatics/bti525 PMID: 16082012

80. Adhikari S., Turner M., & Subramanian S. (2013). Hairpin priming is better suited than in vitro polyadenylation to generate cDNA for plant miRNA qPCR. *Molecular plant*, 6(1), 229–231. https://doi.org/10.1093/mp/sss106 PMID: 23024207

81. Charif D., & Lobry J. R. (2007). SeqinR 1.0–2: a contributed package to the R project for statistical computing devoted to biological sequences retrieval and analysis. In *Structural approaches to sequence evolution* (pp. 207–232). Springer, Berlin, Heidelberg.

82. Camacho C., Coulouris G., Avagyan V., Ma N., Papadopoulos J., Bealer K., et al. (2009). BLAST+: architecture and applications. *BMC bioinformatics*, 10(1), 1–9. https://doi.org/10.1186/1471-2105-10-421 PMID: 20003500

83. R Core Team, R. (2019). R: A language and environment for statistical computing.

84. Wickham, H. (2016). ggplot2: elegant graphics for data analysis. springer.

85. Kassambara, A. (2017). ggpubr: "ggplot2" based publication ready plots. R package version 0.1. 6.

86. Tian T., Liu Y., Yan H., You Q., Yi X., Du Z., et al. (2017). agriGO v2. 0: a GO analysis toolkit for the agricultural community, 2017 update. *Nucleic acids research*, 45(W1), W122–W129. https://doi.org/10.1093/nar/gkx382 PMID: 28472432

87. Kumar S., Stecher G., & Tamura K. (2016). MEGA7: molecular evolutionary genetics analysis version 7.0 for bigger datasets. *Molecular biology and evolution*, 33(7), 1870–1874. https://doi.org/10.1093/molbev/msw054 PMID: 27004904

88. Bodenhofer U., Bonatesta E., Horejš-Kainrath C., & Hochreiter S. (2015). msa: an R package for multiple sequence alignment. *Bioinformatics*, 31(24), 3997–3999. https://doi.org/10.1093/bioinformatics/btv494 PMID: 26315911

89. Nei M., & Kumar S. (2000). Molecular evolution and phylogenetics. Oxford university press.